**Response to Reviewers** (reviewers' comments in italics)

We would like to thank the reviewers for their constructive and detailed feedback. We have substantially revised the manuscript in response to the comments provided and believe that the current version is much improved.

Both reviewers commented (i) on our methodology to constrain the ice flux from calving, as well as (ii) on the lack of support for the melt estimates (since we largely relied on a then yet-to-be-published study). We have addressed these issues as follows:

i) We provide more detail now on the assumptions that go into the calving estimates and highlight the associated uncertainties. Following the suggestions of the reviewers we now calculate the calving flux as a residual of the other terms in the flux balance and discuss the associated uncertainty by comparing it to the independent estimate obtained from the pressure sensor data. We further have added error bars to the plots.

ii) The paper by Slater et al from which the melt estimated are derived has since been published at Geophysical Research Letters and can be accessed here: https://agupubs.onlinelibrary.wiley.com/doi/10.1029/2018GL080763. We have also included more detailed descriptions of the melt modeling efforts in the manuscript, to ensure that it is a stand-alone piece of work. We have further placed the study more carefully in context of the existing literature on melt modeling.

We have also restructured the paper somewhat to more closely reflect the standard sequence of intro, methods, results, discussion, conclusion, as recommended by the reviewers.

Below we respond to each of the individual comments by the reviewers.

**Reviewer #1**

*This study uses field data, satellite observations, and numerical modeling results to investigate spatial variations in iceberg calving and submarine melting. This knowledge is useful because it provides information on how submarine melting might affect calving and terminus retreat. I think this is an interesting way of thinking about the ice-ocean interface.*

*The paper essentially boils down to an analysis of a mass continuity equation (eq. 1 in the manuscript), in which the rate of terminus retreat is related to the glacier velocity, calving rate, and submarine melt rate.*

*The left-hand side of equation 1 contains the ice thickness, the rate of retreat, and the ice velocity. These quantities were determined using fairly traditional methods, and as such I feel confident in the results. I have much more trouble with the right-hand side of equation 1, which contains the submarine melt rate and calving rate.*

We agree with the reviewer that the right-hand side of eq 1 (i.e. the melt and calving terms) is less well constrained than the left-hand side. At the same time understanding the partitioning of melting at calving fronts is key to improving our ability to understand and predict future ice sheet change. Here, we use a unique data set and strive to estimate the relative contribution of melting and calving along the entire glacier for the first time. We are aware of the uncertainties and have made every effort to spell these out, especially in the revised manuscript. At the same time, we feel that the results presented – large spatial variability along the glacier and dominance of calving versus melting – are sound results that are supported by the evidence presented even when the uncertainties are taken into account.

*Specifically:*

*1. The submarine melt rate was determined by some combination of hydrographic observations and numerical modeling. How this was done is not clear, as the modeling is apparently presented in a separate paper that is in review. Without access to that paper and very little description of the model, I am basically asked to take the model results at face value. Even if the modeling paper was already published I would still appreciate to have more details of the model in this paper.*

We thank the reviewer for raising this point. As mentioned above, the paper by Slater et al has since been published and can be accessed here: https://agupubs.onlinelibrary.wiley.com/doi/10.1029/2018GL080763.
We have further added a more detailed discussion of the melt-rate estimation, as well as a melt-specific figure (Fig 5), which will allow for an independent assessment of the melt-rate modeling results. The present manuscript thus becomes a stand-alone piece of work. The added section on melt reads as follows:

"Submarine melt rates at Saqqarliup Sermia during summer 2013 have been estimated by Slater et al. (2018). Here we provide only a brief overview of the approach and build on the results of Slater et al. (2018) to investigate the glacier's flux balance. Melt rates within the two plumes were estimated using standard buoyant plume theory (Jenkins, 2011; Carroll et al., 2016; Slater et al., 2016). Melt rates outside of the plumes were estimated using a high-resolution numerical model of the fjord in the Massachusetts Institute of Technology general circulation model (MITgcm), which has become the leading model for simulating the circulation and water properties of glacial fjords and for estimating the resulting submarine melt rates (e.g. Xu et al., 2012; Sciascia et al., 2013; Cowton et al., 2015; Carroll et al., 2015). Both buoyant plume theory and MITgcm were forced with runoff from the regional climate model RACMO and initialized with hydrographic profiles from the fjord. Slater et al. (2018) also presented observationally-inferred melt rates using water property and velocity measurements collected within 100 m of the calving front. In each approach, Slater et al. (2018) then used the standard three-equation melt rate parameterization of Holland and Jenkins (1999) to convert the modeled or observed water properties and velocities to an estimated submarine melt rate. There is good agreement between the melt rates estimated with MITgcm and with observations (Slater et al., 2018, their Fig 3). Here, we only consider the modeled melt rates (Fig 5), which have the advantage of covering the

whole extent of the glacier front (unlike rates inferred from observations, which have data gaps in and around the plumes).

There is large spatial variability in submarine melt rates along the glacier front (Fig 5). Submarine melt rates are highest (both in a depth-averaged and maximum sense) within the two plumes where the discharge of buoyant surface meltwater from beneath the glacier gives high water velocities. Outside of the two plumes melt rates are much smaller in a depth-averaged sense, however the lateral circulation excited by the plumes combines with warm surface waters to give high melt rates near the surface outside of the plumes (Fig 5c; Slater et al., 2018).

While these melt-rate estimates represent the state-of-the-art in terms of melt-rate modeling, we stress that they are based on a melt-rate parameterization that has not been confirmed by observations, especially for the case of a mostly vertical front of a tidewater glacier. The uncertainty associated with these melt-rate estimates is further discussed in Section 5."

*2. The calving rate was estimated by (i) locating calving events with measurements of ocean waves and (ii) converting measurements of calving events into calving rates by somehow scaling the number of events (and amplitude of the waves) so as to roughly balance equation 1. Given the wide variety of types of calving events and iceberg geometries and poor understanding of wave generation by calving events, it seems dangerous to assume any relation between wave amplitude and calving event size. Using this method, the authors are unable to close the mass budget (see Fig. 6c) along the southern part of the terminus, which they attribute to the style of calving that they observe there. That's fine, I suppose, but elsewhere along the terminus the left- and right-hand sides of equation 1 differ by a factor of 2 or more, which raises questions about the validity of their results — and in particular the modeled melt rates and the estimated calving rates.*

We thank the reviewer for this feedback. We appreciate that there are large uncertainties associated with the calving term and that this makes it difficult to balance the mass flux at the terminus. In the revised version of the manuscript we have therefore put much of the weight of our argument on the perspective of computing the calving flux as the residual from the other three terms in the flux balance equation (see also next comment).

However, the calving estimates from the pressure sensor data provide insightful independent results regarding the spatial distribution of the frequency and (to a more limited extent) the volume flux due to calving. Overall, the combination of calving data and melt flux data is unique and it provides at least rough estimates for all terms in eq 1. Our results highlight the challenges of balancing the mass flux, even when ocean and calving conditions are known, and emphasize the need to reconcile commonly accepted melt rate estimates with the spatial variability across the front.

We agree that a relation between wave amplitude and calving event size should be adopted with great caution. However, to a first rough approximation, it might be assumed that larger calving events are correlated with larger wave amplitudes. The two main characteristics that can skew this direct correspondence are the geometry of the calving block (is it an efficient wave-generator or not) and the height from which it falls. If certain

regions or times produce calvings that are more efficient wave generators than the average this would lead to an overestimation in calving volume for those regions or times. The same applies to calving heights, as illustrated in the promontory: here we know that the high cliffs produce frequent (but small) calvings from great heights which leads to a spuriously elevated volume flux in this region. For the main part of the glacier, however, it may be a satisfactory first approximation that geometries and heights are roughly evenly distributed so that we can statistically expect that larger calving events are correlated with larger wave amplitudes.

However, such a relationship is indubitably speculative. For the final flux balance estimates we therefore invoked the simpler approximation that for the main part of the glacier higher calving frequencies correspond to higher calving fluxes. This led us to use a scaled frequency of calving events as an estimate for calving volume, thus eschewing the added uncertainties that come with trying to draw conclusions from the wave amplitudes (as pointed out by the reviewer). This is further supported by the result that the calving volume as estimated using wave amplitudes (black line in Fig 5b) is spatially correlated with the observed calving frequency (red bars in Fig 5b), i.e., the size of calving events appears to be fairly uniformly distributed along the glacier front.

We have aimed to emphasize these caveats and clarify the limitations associated with the calving data at several places in the manuscript, and particularly in the following revised paragraph:

"Even though this dataset presents a rather accurate record of calving frequencies, it remains challenging to infer a total volume of calved ice (Minowa et al., 2018). This is due to the different modes of calving (e.g., ice-cliff calving versus submarine calving), as well as the different shapes of calved ice blocks and the differing heights from which they fall (or depths from which they rise). Distinguishing between these events from the pressure sensor data is a difficult task and beyond the scope of this study. The pressure sensors do record an amplitude of the incoming wave packet associated with a given calving event. Crudely approximating that this amplitude is proportional to the size of the calved ice we can estimate a relative calving volume (black curve in Fig 6b). However, since a small cone-shaped ice block can act as a more efficient wave generator than a large flat piece of ice (N. Pizzo, personal communication, Bühler, 2007), it is difficult to ascertain a direct relation between wave amplitudes and calving volume. In what follows we therefore only consider the calving frequency record and will scale this record such that the resulting calving flux approximately closes the mass budget at the glacier front (see Section 4.2). Given the limitations of the data, we take such a scaling to be the most justifiable first-order approximation, supported by the rather uniform distribution of estimated calving event sizes along the glacier front. The scaling factor is chosen such that the mean calving volume is equal to the mean of the residual, i.e. $\langle C \rangle = \langle H(R + vi) - DM \rangle$."

*It's not clear to me why the calving rate wasn't just calculated by subtracting the melt rate from the left-hand side of equation 1, which would at least ensure that mass is being conserved. Nonetheless, a major conclusion in the paper is that frontal ablation is dominated by melting in a couple of specific locations but is otherwise dominated by calving. That is an interesting result, but I think that point can be made much more simply, without the need to convert wave amplitudes to calving event sizes, and may*

*already be apparent in the modeling paper that is in review. For example, in figure 6b it is apparent that the modeled melt fluxes are highly focused on certain regions of the terminus, which already implies that the calving fluxes must be comparatively large everywhere else.*

We thank the reviewer for this comment and have added the suggested calculation to the manuscript: we now provide an estimate of the calving flux (per unit width) as the residual of the other three terms in eq 1. This is shown in the revised Fig 7c. The two methods compare well in terms of magnitude of the calving flux except in the area of the promontory where the elevated cliff heights lead to a different calving regime with frequent smaller calving events from greater heights, as discussed above and in the text.

We maintain that the calving flux as estimated from observations is a valuable addition here, since it provides an independent estimate, and highlights possible issues with the modeled melt-rates: the calving distribution along the glacier front is more homogenous than the extremely localized melt rates would suggest. We conclude from this result that conventional melt rates should be revisited. This is discussed in more detail in the revised manuscript in section 5.1.

*I include some detailed comments below, focusing on areas where I found the descriptions to be somewhat ambiguous. In addition, all errors are discussed in the text, I think it would be helpful to include error bars or confidence intervals in the figures (especially figure 6).*

We thank the reviewer for the comments above as well as the specific comments below, which we have addressed to our best ability.

Error bars have been added to Figures 3 and 7 (formerly Fig 6). Quantifying the uncertainty in the melt rates is somewhat challenging, since there are uncertainties associated with the melt parameterization themselves, as well as with the model and observations. We have expanded our discussion of the uncertainties inherent in the melt rate estimation as follows:

"The finding that calving appears to make up almost the entire loss of ice is somewhat unexpected, in particular since during the study period the glacier's calving activity was limited to relatively small events, and the fjord was by-and-large devoid of icebergs. Furthermore, the melt rates used here are roughly double that of what previous estimates would have been since we account for additional melt that arises from the recirculation of warm ambient surface waters (Slater et al., 2018). Yet, melting supposedly only makes up ~6% of the total ablation.

Given the lack of observational verification of the current melt rate parameterization, it is worth considering end-member melt rate scenarios. Perhaps the key parameter in the melt rate parameterization is the thermal Stanton number, which directly controls the rate of transfer of heat from the ocean to the ice. Its canonical value is based largely on field observations at a cold Antarctic ice shelf and there are as yet no strong observational constraints from tidewater glaciers. Furthermore, Ezhova et al. (2018) have recently argued for a larger Stanton number based on direct numerical simulations. We thus consider lower and upper bounds for melt rates in which the thermal Stanton number is respectively reduced and increased by 50% (Fig 7b,c).

To obtain the upper bound melt rate scenario, we also increase the outside-of-plume water velocity which enters the melt rate parameterization. While vertical velocities inside of plumes might be considered reliable based on well-validated plume theory (Morton et al., 1956), one could argue that the mean modeled outside-of-plume velocities may be too small for a number of reasons including coarse model resolution and the lack of tides, surface waves, and calving events which may excite water motion. These factors might crudely be taken into account by placing an additional velocity in the melt-rate parameterization. Such an approach has some precedent with the inclusion of tides beneath ice shelves (Jenkins and Nicholls, 2010). In the upper bound melt rate scenario, we thus add 0.2 m/s to the outside-of-plume water velocity entering the melt rate parameterization.

In the lower bound melt rate scenario, melting accounts for an even smaller fraction of mass loss than in our best estimate, but is still significant inside the plumes. In the upper bound melt rate estimate, melting accounts for a significant proportion of mass loss both inside and outside of the plumes (Fig 7b). Clearly this is an observationally under-constrained discussion, and we emphasize that these upper and lower bounds are very rough error estimates as the state of understanding of submarine melting does not yet permit rigorous quantitative assessment of uncertainties. Yet these bounds do show that through reasonable modification of the melt rate parameterization, melting can account for a larger fraction of the ice loss than reported in our best estimate. Even by introducing these uncertainties, however, the analysis presented still indicates that calving is the dominant mode of mass loss for most of the glacier front (except at the localized melt plumes)."

***Specific comments:***

***p. 1, l. 14:*** *Tidewater glaciers aren't boundaries per se but rather a part of the ice sheet. Also, tidewater glacier termini (and the bottom of the remaining ice shelves) are really the only boundary between the Greenland Ice Sheet and the ocean.*

We thank the reviewer for this comment and have adjusted the text to simply read:

"Tidewater glaciers act as thermodynamic buffers as well as mechanical buttresses between the ocean and the Greenland ice sheet (Rignot and Thomas, 2002; Howat et al., 2007; Nick et al., 2009)."

***p. 2, l. 1-2:*** *Its a little confusing how these sentences jump from ablation (in general) to specifically talking about frontal ablation.*

We have added 'frontal' to the first use of 'ablation' for better clarification.

***p. 2, l. 15:*** *You could also mention that ocean surface gravity waves (both shortand long-period) have been used to observe calving events in Greenland in previous studies.*

This has been added, together with a reference to Minowa et al (2018).

***p. 2, l. 26:*** *It wasn't clear to me how the hydrographic data was used to infer melt /*

*constrain the submarine melt model.*

We thank the reviewer for this comment — this is now discussed in more detail in Section 3.3 (see general comments above).

***p. 4, l. 1:*** *In what way is the plume amplified? The drainage event is relatively shortlived, so I suspect it wouldn't have an impact on the plume over time-scales longer than about a week.*

We thank the reviewer for this comment and have changed the text to read:

"While this plume appears to be an annually recurring feature, its discharge is likely amplified episodically by the cyclical drainage of the large ice-dammed lake Tininnilik located to the south-west of the promontory (Kjeldsen et al 2017)."

***p. 4, l. 28:*** *Did you correct the DEM to account for the difference between the ellipsoid and the geoid?*

Here we set the reference height at the estimated current sea level as measured by the DSM a few hundred meters from the terminus (so as to avoid bleed-in effects from the ice—ocean boundary), and we measure the height of the glacier as simply the difference between the estimated sea surface and the height of the ice at the glacier front (i.e., we only consider relative, not absolute, heights).

***Figure 2, caption:*** *It doesn't really make sense to talk about the flux being into the page here. Do you mean that the velocity profile is from the perspective of somebody looking down glacier?*

We thank the reviewer for this suggestion. The text has been changed to read:
"Here, as in all figures, the orientation is looking down-glacier."

***p. 5, l. 11:*** *Speculation shouldn't be part of the methods section.*

We appreciate the reviewer's point, and have moved this paragraph to later in the text. Note, however, that we did not structure the paper with a strict methods—results—discussion layout (so as to tell the story in a more streamlined way) and the discussion of the potential partial flotation of the terminus remains in the section that estimates the ice advection.

***Figure 3b*** *(and elsewhere): I'm not sure if its correct to refer to this quantity as a flux. Should it be a flux per unit width?*

We thank the reviewer for highlighting this inconsistency — it should indeed be flux per unit width. The text has been changed accordingly.

***p. 7, l. 7:*** *You can be more specific here. For an infinite slap with no sliding and uniform temperature, the depth-averaged velocity is 80% of the surface velocity. The percentage goes up for rapidly sliding glaciers and those that have concentrated deformation at depth, such as tidewater glaciers.*

We thank the reviewer for this suggestion and have adjusted the manuscript to read:

"This assumes plug flow, i.e., that the ice velocity is approximately constant from the surface to the ice—bedrock interface. Note that for a glacier with no sliding and uniform temperature, the depth-averaged velocity is 80% of the surface velocity. For fast-flowing tidewater glaciers with concentrated deformation at depth, such as Saqqarliup, plug flow is therefore considered a good approximation (Meier and Post, 1987)."

***Figure 4c:*** *For clarity, considering specifying that negative retreat rates indicate advance. (My personal preference is to plot dL/dt, so that positive indicates advance and negative retreat, but this is fine too.)*

We thank the reviewer and have added the following:

"Here, positive *R* represents glacier retreat and negative *R* glacier advance."

***p. 8, l. 9:*** *Don't you mean across-glacier variability?*

We thank the reviewer for pointing out this source of confusion. We have changed the text to read:

"However, there is substantial variability along the glacier front in this cycle."

***p. 9, l. 1-2:*** *Do you actually calculate the retreat rate perpendicular to the initial terminus, or is it perpendicular to a straight line fit through the initial terminus?*

Yes, it is indeed perpendicular to the initial terminus, which we felt was a more rigorous estimate since parts of the southern section of the terminus are at an acute angle to the main glacier front and a small retreat in those regions can lead to spuriously large retreat when considering a straight line fit.

***p. 9, l. 8-14*** *(and elsewhere in the paper): "rates" and "fluxes" are conflated in several places, which may be confusing. For example, in equation (1), H*R is not the retreat rate.*

We thank the reviewer for pointing out this accuracy and have strived to be more precise in our uses of the terms "rates" and "fluxes" in the revised version of the manuscript.

***p. 9, l. 25:*** *derived calving record by: : : ? Should "by" be deleted? Or is something missing here?*

Yes, "by" has been deleted.

***p. 10, l. 16:*** *How do you do this scaling? Through a minimization procedure?*

This is correct. The calving frequencies are scaled such that the resulting mean calving flux per approximately balances the flux over the main part of the glacier. Corresponding text has been added to the manuscript to clarify this point:

"The scaling factor is chosen such that the mean calving volume is equal to the mean of the residual, i.e. $\langle C \rangle = \langle H(R + v_i) - DM \rangle$."

***p. 10, l. 13-15:*** *Laboratory experiments by Burton et al. (2012) suggest that the wave amplitude of waves produced by capsizing icebergs depends on the energy released during the capsize event, which scales nonlinearly with iceberg geometry.*

We thank the reviewer for pointing us to that result. The link between iceberg capsizing and calving events is interesting, but it is difficult to ascertain how the nonlinearity for iceberg capsizing translates to calving, and we have therefore chosen to eschew a discussion of this question in the paper.

***p. 10, l. 24:*** *I assume that the modeled melt rates are constrained by hydrographic observations. Is that correct?*

This is correct. We have clarified this in the revised manuscript as follows:

"Both buoyant plume theory and MITgcm were forced with runoff from the regional climate model RACMO and initialized with hydrographic profiles from the fjord. Slater et al. (2018) also presented observationally-inferred melt rates using water property and velocity measurements collected within 100 m of the calving front. In each approach, Slater et al. (2018) then used the standard three-equation melt rate parameterization of Holland and Jenkins (1999) to convert the modeled or observed water properties and velocities to an estimated submarine melt rate. There is good agreement between the melt rates estimated with MITgcm and with observations (Slater et al., 2018, their Fig 3). Here, we only consider the modeled melt rates (Fig 5), which have the advantage of covering the whole extent of the glacier front (unlike rates inferred from observations, which have data gaps in and around the plumes)."

***p. 12, l. 21:*** *Doesn't the thickness have to go to 0 at the margins?*

We thank the reviewer for raising this point. We have added "Away from the margins, …" to clarify our statement.

***p. 12, l. 29-30:*** *Seems self-evident to me.*

We agree with the reviewer and have replaced "which suggests that" with "since".

***p. 14, l. 4-5:*** *Can you quantify the amount of ice in the fjord and how it varies seasonally (even in a rough sense by looking at satellite imagery)? This glacier is pretty slow, so the calving fluxes would have to be pretty small.*

We agree with the reviewer that helpful insights may be gained from looking at the volume of ice in the fjord. However, the estimation of seasonal variations is made difficult by the lack of wintertime data and also the presence of sea ice in the fjord for much of the year. We feel that such estimates would go beyond the scope of the present study.

**Reviewer #2**

*Overall I think this is an interesting paper. It's a tricky topic, but an important one, and so it is nice to see people try to improve our knowledge. However, I do have a couple of major concerns about the fundamental approach. The authors are essentially trying to determine the balance between ice losses from calving and those from melting. However, it seems to be that both of these things are poorly constrained:*

*The melt rates are calculated using a model and observations, but these are from Slater et al., which is currently 'submitted'. As such, it is not accessible to me and I also think it is inappropriate to treat this as accepted, when it hasn't been peer-reviewed. I'm not saying this is the case, but if Slater et al were to be rejected or the technique deemed in appropriate, it would mean that this paper also had the same issues.*

We share the reviewer's concerns and are grateful for this feedback. The paper by Slater et al. has since been published at Geophysical Research Letters and is available here: https://agupubs.onlinelibrary.wiley.com/doi/10.1029/2018GL080763.
We have further expanded the discussion of the melt rate estimation such that the present work is a stand-alone unit. Please also see our response to the similar comment of Reviewer #1 on page 1 of this document.

*The other term is calving, for which the authors have frequency (which is a useful dataset) but no volume / area data. They therefore take it as the residual of the left hand side of the equation, minus melting. As noted above, the melt calculations may have quite high errors and the method is actually not published. As such, I think this limits the confidence we can have in the results.*

In the revised version we estimate calving flux both as the residual of the other terms in eq 1 (as also suggested by Reviewer 1) and by using the independent (scaled) measured calving frequencies. This sheds some more light on the uncertainty associated with our calving estimates. Furthermore, we believe that the more robust justification of the melt estimates in the revised manuscript (and the publication of Slater et al., GRL, 2018) will provide better support for our discussion of the calving flux estimates.

*The approach of using waves to ID calving events has been demonstrated in Minowa et al 2018 but they also had time-lapse imagery, which meant they could determine the type of calving (topple etc) and they did not need size. Here, I think the size is needed, so that the calving term is more robust.*

We fully agree that the knowledge of either the type of calving or the size of the calved ice would be required to exactly close the mass flux across the terminus. In fact, we do have simultaneous time-lapse imagery for parts of the calving record. (This imagery is of sufficient resolution to validate the accuracy of the pressure-wave detection, but it is not detailed enough to reveal the exact type of calving for individual events, nor the size of the broken-off pieces.) However, during the field experiments we observed that there are two areas of the glacier with markedly distinct calving regimes - the promontory and the main glacier. Within those two regions the calving events appeared more uniform. This is further supported by the fact that the measured wave amplitudes do not highlight

substantial differences in calving energies along the main part of the glacier. We would therefore argue that a scaled calving frequency — even though an imperfect measure — is a helpful first step toward robustly estimating the calving flux along the glacier face.

*A more minor point is the paper structure: the methods and results are mixed together. I'm not totally against this and I can see why the authors have taken the approach here (as you need to get the results from one part to do the next), but I think it does reduce the accessibility for someone trying to repeat the experiments, who just wants to get at the methods. As noted above, I think it needs to at least briefly describe the methods in Slater et al submitted here (to avoid the reader having to go and find another publication). Slater et al should also be through the peer review process before it is cited, as it's central to the argument.*

We thank the reviewer for the comment regarding the structure and have restructured the paper with the more traditional sequence of methods, results, discussion in mind. In the revised version, we provide two combined methods/results sections that present the physical setting and estimates of the 4 terms of the flux balance (Sections 2 and 3). This is followed by two discussion sections (Sections 4 and 5), which discuss the spatial variability and relative importance of melting and calving. Following the reviewer's suggestion, and in light of the discussion above, we have further expanded the discussion of the melt estimates so as to guarantee this paper to be stand-alone.

*Finally, I think the abstract is a bit misleading over time frames. You have the calving data for July, but the earlier material implies that this is a year-round budget.*

We thank the reviewer for raising this point. We have added "in the summer" to the first sentence of the abstract for clarification.

*I've attached some minor comments in the annotated pdf.*

Comments from the annotated pdf:

***p. 1, l. 5:*** *melting-dominated etc.*

This has been fixed.

***p. 1, l. 14:*** *Also Jensen et al 2016. I'd add another paper or two as examples.*

We thank the reviewer for this suggestion. A reference to Jensen et al (2016) has been added.

***p. 1, l. 16:*** *I'd say since the 2000s, as it wasn't consistent - see e.g. Howat et al., 2008 for east Greenland.*

This has been changed accordingly.

***p. 1, l. 18:*** *May want to add Hill EA, Carr JR, Stokes CR. A Review of Recent Changes in Major Marine-Terminating Outlet Glaciers in Northern Greenland. Frontiers in Earth Science 2017, 4, 111.*

We thank the reviewer for this suggestion. A reference to Hill et al (2017) has been added.

***p. 2, l. 13:*** *Might be worth noting that data in fjords are very limited, and the data we have are only from a small number of glaciers (e.g. the Rignot paper on W Greenland, Helheim, Peterman etc) which further impacts our capacity to understand melt rates.*

We thank the reviewer for this suggestion and have adjusted the text to read:

"In-situ ablation data remains scarce, and previous studies of explicit calving activities of Greenland's tidewater glaciers have typically been limited to visible daylight hours […]"

***p. 2, l. 19:*** *I defer to the editor as to whether 'submitted' papers are allowed. Is there not a published paper you can cite here?*

References to Slater et al (submitted), have been changed to Slater et al (2018), as discussed above.

***p. 2, l. 31:*** *Why this glacier? If it's for logistical reasons, there's no issue but I'd just note it.*

We have added the following text for clarification:

"This site was chosen because ocean properties and bathymetry could be measured within 100 m of the ice front. Such observations are exceedingly difficult to obtain at larger glaciers which often have an ice mélange that obstructs access and where calving poses a major threat to equipment and personnel."

***p. 4, l. 1:*** *... to be an annually recurring….*

This has been fixed.

***p. 4, l. 5:*** *we will. Please avid shortenings like this.*

This has been fixed. We apologize for the sloppiness.

***p. 4, l. 9:*** *Which two? Restate the dates*

This has been changed to 'the 2012 and 2013 field seasons'.

***p. 4, l. 11:*** *Spell out acronyms the first time they are used.*

As requested, we have spelled out the acronyms for REMUS, ADCP, NMEA, and XCTD.

***p. 4, l. 11:*** *these data. 'Data' is a plural noun.*

This has been changed.

***p. 4, l. 20-26:*** *This feels more like results than methods. Please make it clear whether this background info from a previous study, needed to understand the methods, or move it to the appropriate place in the results.*

As discussed above, we have attempted to structure the revised article in a more traditional way.

***p. 5, l. 1:*** *Again, seems like results not methods. I looked back and the title of the section includes the physical setting, but it just seems odd having this here, as these are really results to me. Please revise this throughout this section.*

*Reading further on, there doesn't appear to be a results section. Personally, I'd prefer to see separate methods and results sections, as I think it's easier for the reader to access the information they need.*

Please see our response to the comment above.

***p. 6, l. 9:*** *Terms 'stream' and 'drainage location area bit confusing here - I assume you mean where the fast ice flow meets the ocean, but it could be mis-read as a water stream.*

We thank the reviewer for this request for clarification and have changed the text to read "ice stream".

***p. 7, l. 1:*** *Please indicate which months these are.*

We have added "(June—September)".

***p. 7, l. 2:*** *Why is it not shown?*

Please see response to next comment.

***p. 7, l. 2:*** *So is this why you're excluding it? I.e. because this is an 'extreme' event? Please state this.*

We thank the reviewer for highlighting this, and have adjusted the text to read:

"This slowdown is not shown here as it has been linked to a major drainage event of lake Tininnilik (Kjeldsen et al, 2017), and therefore subject to altogether different environmental forcing."

***Figure 5b:*** *This is really interesting information, but the figure is so small I struggle to read it. Please make it bigger so that the dots are easier to see.*

The figure has been revised such that the original sub-figure 5a is now an inset to the former Fig 5b, which in turn is substantially larger now. (This is figure 6 in the revised manuscript).

***p. 8, l. 7:*** *seasonal cycle in terminus position, with a mean advance for the entire front of…..*

We thank the reviewer for this suggestion. The text has been changed accordingly.

***p. 9, l. 20:*** *How Representative do you think this is of the rest of the summer? I think you should make clearer in your abstract that this is a summer balance - if you only have calving events for this period, it can't be a year round balance. It would also be helpful to give this context e.g. do 50% of all calving events in a given year occur in this time or is it 90%?*

We thank the reviewer for this comment and have changed the beginning of the abstract to clarify that we are looking at the summer months only. It is difficult to estimate how much of a year's calving activity occurs during the summer, since there is close to no data of wintertime conditions. We believe that such an estimate is beyond the scope of this study.

***p. 10, l. 1:*** *This is an interesting point, as I would expect the calving frequency to be highest where the glacier is thickest (and deepest bed).*

We agree with the reviewer.

***p. 10, l. 29:*** *Are these your results or Slaters? If the former, please show them. Might be helpful to add the figure either way, so the reader can easily refer to it.*

A melt figure, using data from Slater et al (2018), has been added (Fig 5).

***p. 15, l. 29:*** *This has been observed on a larger scale for lake-terminating glaciers in New Zealand. E.g. Robertson et al 2013.*

We thank the reviewer for this suggestion and have added references to Robertson et al (2012), as well as the review by Benn et al (2017).

# Large spatial variations in the ~~frontal mass budget~~ flux balance along the front of a Greenland tidewater glacier

Till J. W. Wagner[1], Fiamma Straneo[2], Clark G. Richards[3], Donald A. Slater[2], Laura A. Stevens[4], Sarah B. Das[5], and Hanumant Singh[6]

[1]Department of Physics and Physical Oceanography, University of North Carolina Wilmington, NC 28403, USA
[2]Scripps Institution of Oceanography, University of California at San Diego, La Jolla, CA 92093, USA
[3]Bedford Institute of Oceanography, Fisheries and Oceans Canada, Dartmouth, NS B2Y 4A2, Canada
[4]Lamont-Doherty Earth Observatory, Columbia University, Palisades, NY 10964, USA
[5]Department of Geology and Geophysics, Woods Hole Oceanographic Institution, Woods Hole, MA 02543, USA
[6]Department of Electrical & Computer Engineering, Northeastern University, Boston, MA 02115, USA

**Correspondence:** Till J. W. Wagner (wagnert@uncw.edu)

**Abstract.** ~~We investigate the frontal mass budget~~

The frontal flux balance of a medium-sized tidewater glacier in western Greenland ~~. This is done by comparing the seasonal retreat of the glacier to ice advection and ablation along the front. Frontal ablation is partitioned into calving~~in the summer is assessed by quantifying the individual components (ice flux, retreat, calving, and submarine melting~~, both of which are estimated from in situ observations . We observe~~ ) through a combination of data and models. Ice flux and retreat are obtained from satellite data. Submarine melting is derived using a state-of-the art high resolution ocean model informed by near-ice observations and calving is estimated using a record of calving events along the ice front. All terms exhibit large spatial variability ~~in all mass budget terms along the glacier front. In particular, we find that~~ along the ~~ablation of the glacier frontis characterized by two main regimes: melting dominated versus calving dominated. While melting-dominated segments appear to be associated with subglacial discharge plumes, calving-dominated regions occur outside such plumes. The melting-dominated segments are rather localized, and the majority of ablation is estimated to occur in the form of calving. However, we stress the large uncertainty in melt rate estimates and consider the possibility that current parameterizations substantially underestimate melting~~ ~ 5 km wide ice front. It is found that submarine melting accounts for much of the frontal ablation in small regions where two subglacial discharge plumes emerge at the ice front. Away from the subglacial plumes, the estimated melting accounts for a small fraction of frontal ablation. Glacier-wide, these estimates suggest that mass loss is largely controlled by calving. This result, however, is at odds with the limited presence of icebergs at this calving front - suggesting that melt rates in regions outside of the subglacial plumes may be underestimated. Finally, we argue that localized melt incisions into the glacier front can be significant drivers of calving. Our results suggest a complex interplay of melting and calving marked by high spatial variability along the glacier front. ~~Understanding the impact of such local variability on larger scale ice dynamics may help guide future mass balance projections for tidewater glaciers.~~

## 1 Introduction

The retreat of Greenland's tidewater glaciers may be among the most noticeable manifestations of a changing global climate ~~(Carr et al., 2017)~~(Jensen et al., 2016; Carr et al., 2017). Tidewater glaciers ~~present an important boundary between the ocean and the Greenland ice sheet; they~~ act as thermodynamic buffers as well as mechanical buttresses between the ocean and the main Greenland ice sheet (Rignot and Thomas, 2002; Howat et al., 2007; Nick et al., 2009). The speed-up of the Greenland ice sheet observed since the ~~year 2000~~ early 2000s (Howat et al., 2008; Moon et al., 2012) has likely been caused (at least to some degree) by the thinning of the glaciers' termini (Vieli and Nick, 2011) and, in some cases, the disappearance of their floating tongues ~~(Holland et al., 2008; Wilson et al., 2017)~~(Holland et al., 2008; Wilson et al., 2017; Hill et al., 2017). The processes that determine the flux balance at the glacier front therefore impact the ice sheet as a whole, yet a comprehensive understanding of these processes remains elusive. Increased ocean and air temperatures are expected to further increase the rates of glacier retreat in the coming decades (Joughin et al., 2012; Nick et al., 2013), lending additional weight and urgency to the study of calving front dynamics.

For a retreating glacier, the delivery of upstream ice to the terminus is outweighed by the loss of ice due to frontal ablation. At tidewater glaciers this frontal ablation occurs predominantly through two distinct processes: submarine melting and calving~~.~~ ~~The submarine melting of the glacier front – "melt" hereafter – is a continuous (though seasonally varying) process, determined largely by the~~ , both of which remain very difficult to constrain observationally. Recent studies have reported ways to measure submarine melting either directly (from repeat multibeam sonar surveys Fried et al., 2015), or indirectly (by considering the ocean heat tra . In most cases, however, melt is estimated using parameteriziations which require local ocean temperatures and water velocities ~~(Holland and Jenkins, 1999; Jackson and Straneo, 2016). The main challenge in constraining~~ (Holland and Jenkins, 1999). Constraining melt rates at glacier fronts ~~therefore lies in measuring~~ then relies on accurate observations of the ocean properties at these hard-to-reach ice–ocean interfaces ~~, and~~ and on finding appropriate parameterizations that translate these observations to melt rates. The continued scarcity of ~~such observations~~ near-terminus data results in large uncertainties in current melt parameterizations (Straneo and Cenedese, 2015).

~~Calving, by contrast, is a discontinuous and highly complexprocess which is~~ While melting is a continuous process, calving is discontinuous, highly complex, and influenced by a multitude of environmental factors, as well as the condition of the ice itself (Benn et al., 2007). In recent years, much effort has been dedicated to studying the calving of tidewater glaciers (see the review by Benn et al., 2017), yet a comprehensive understanding of what processes and variables determine the frequency and magnitude of calving events remains elusive.

Oftentimes calving and melt fluxes are not considered separately, but rather as a single ablation term, in particular when derived from satellite imagery (Luckman et al., 2015). ~~Previous~~ In-situ ablation data remains scarce, and previous studies of explicit calving activities of Greenland's tidewater glaciers have typically been limited to visible daylight hours (see, for example, the calving event catalogue of Åström et al., 2014), or somewhat indirect detection methods such as teleseismicity (Veitch and Nettles, 2012) and measuring calving-generated surface gravity waves (Minowa et al., 2018).

Finally, the calving and melt fluxes of glaciers are oftentimes described by single (horizontally and vertically-averaged) mean values (Rignot et al., 2016). However, both melting and calving can vary substantially along the front of a glacier, with largely unknown implications for the overall stability of a glacier front. For example, submarine melt is enhanced ~~by an order of magnitude~~ in the vicinity of subglacial discharge plumes~~(?)~~, leading to pronounced undercutting and ~~incision~~ incisions into the ice front (Fried et al., 2015). Spatially resolving these differences is challenging, and in particular spatial calving distributions are difficult to obtain.

Here we use a multifaceted dataset ~~to quantify~~ for a first attempt at quantifying the relative contribution of calving and melting and their spatial variability along a glacier front. The dataset consists of both in-situ and remotely-sensed observations of the front of Saqqarliup Sermia, a mid-sized Greenland tidewater glacier. The ~~data~~ dataset is unique in its detail, close proximity to the glacier front, and in that it contains observations of all of the main physical quantities of interest. The dataset consists of (i) detailed bathymetry at the glacier front, (ii) high-resolution ice-surface elevations, (iii) InSAR-derived ~~ice-velocities~~ ice velocities at and upstream from the glacier front, (iv) a continuous 3-week calving event catalogue, (v) local hydrographic measurements that allow for estimates of melt rates, and (vi) multibeam sonar imagery of the underwater shape of the glacier front. The spatial and temporal concurrence of these observations allows us to compare and contrast the individual components that make up the frontal mass budget of the glacier.

Specifically, we first derive ice flux and retreat using satellite data collected over the observational period. We then compute submarine melting using a numerical model that is constrained (and validated) by near-ice hydrographic observations. Next, we estimate calving as a residual of the other terms in the frontal mass budget and compare this estimate with the observed calving frequencies. Finally, we bring our findings together to assess the overall mass budget and discuss how calving may be enhanced by highly focused melt "hotspots".

## 2 Field campaigns and physical setting

Saqqarliup Glacier and the adjacent Sarqardleq Fjord were visited during two field seasons in the summers of 2012 and 2013. This site was chosen because ocean properties and bathymetry could be measured within 100 m of the ice front. Such observations are exceedingly difficult to obtain at larger glaciers which often have an ice mélange that obstructs access and where calving poses a major threat to equipment and personnel. The fjord is a tributary to the Ilulissat Icefjord, with the north-west facing front of the glacier (Fig 1) located 30 km south-east of Ilulissat Icefjord. At the glacier front, the fjord is about 5 km wide and the terminus is mostly, if not completely, grounded.

Since 2004, the main north-eastern part of the ~~glacier~~ terminus has been retreating more rapidly than the south-western section, which now juts out by almost 1 km from the rest of the glacier front (Fig S2). This part of the glacier, which we refer to as the ~~"promontory"~~ "promontory" (Fig 1), is grounded in shallow bathymetry and features tall ice cliffs (40–50 m above mean sea level, see Section 2.2). Overall, the glacier advanced slightly between 1975 and the ~~mid-1990s~~early 1990s, but experienced an accelerating retreat from the mid-1990s until 2016 (Fig S2; Stevens et al., 2016). The front position has been relatively stable from 2016 to 2018.

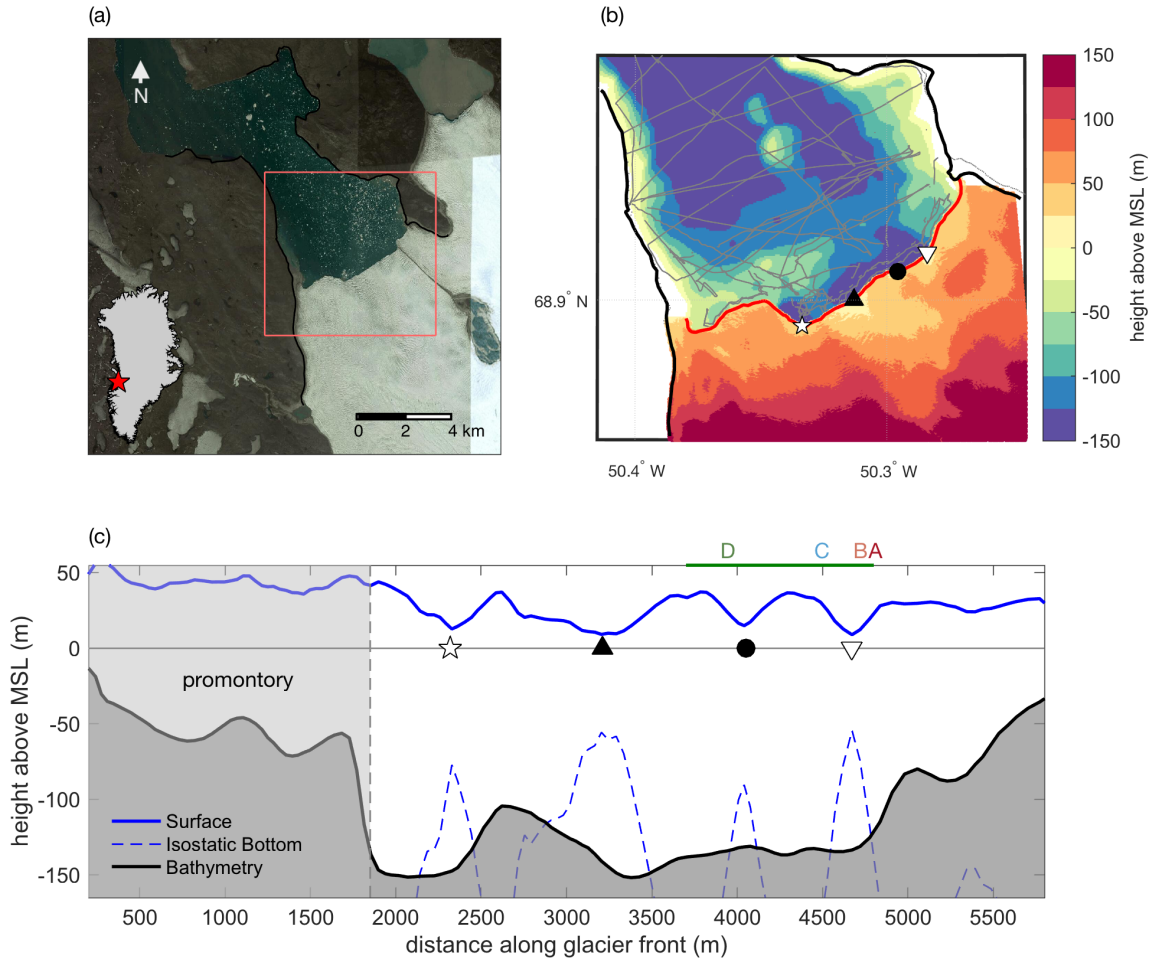


**Figure 1.** (a) Landsat-8 image of the lower part of Saqqarliup Sermia, and Sarqardleq Fjord. The inset of Greenland shows the location of the glacier. (b) Gridded bathymetry from in-situ observations (readings indicated by gray dots). Also shown is the surface height from ArcticDEM (Digital Elevation Map created by the Polar Geospatial Center from DigitalGlobe, Inc. imagery). Red line shows the front position on 9 July 2013. (c) Surface height (blue) and bathymetry (black) along glacier front (following the red line in panel b). Also shown is the isostatic bottom of the ice (blue dashed). Locations of two main plumes are highlighted in panels (b) and (c) by ☆ and ▽; two additional surface dips are indicated by ▲ and ●. The green horizontal line above panel (c) and the letters A-D indicate the locations of the front profiles shown in Fig 8.

The 2012 survey, described by Stevens et al. (2016), revealed the presence of two main subglacial discharge plumes along the glacier front which, in turn, drained the two dominant catchment basins. The plume entering the fjord at the eastern edge of the promontory (Fig 1) has an order of magnitude greater drainage and can result in an outcropping surface pool (Mankoff et al., 2016). We refer to this as the ~~“~~"main" plume. While this plume appears to be ~~a yearly~~ an annually recurring feature, ~~it~~

its discharge is likely amplified ~~in some years~~ episodically by the cyclical drainage of the large ice-dammed lake Tininnilik located to the south-west of the promontory (Kjeldsen et al., 2017). We note that the dramatic retreat of the glacier front in 2015 coincided with a major drainage event of lake Tininnilik (Kjeldsen et al., 2017). The second recurring plume, which we will refer to as the "secondary" plume, is located closer to the north-eastern margin of the glacier (Fig 1)~~, which we'll refer to as the "secondary" plume~~.

In what follows, we use bathymetry data from both years, while the other in-situ observations were mostly collected during the 2013 season (see Stevens et al., 2016; Mankoff et al., 2016, for further details on the field campaigns).

### 2.1 Bathymetry

The bathymetry of Sarqardleq Fjord was first mapped in detail during ~~these two~~ the 2012 and 2013 field seasons and the immediate bay in front of the terminus was found to feature depths of 40 – 150 m (Stevens et al., 2016). These initial results were limited to data from ~~REMUS and~~ a Remote Environmental Monitoring UnitS (REMUS) Acoustic Doppler current profiler (ADCP) and a shipboard ADCP, which did not get closer than ~ 200m to the glacier front. Here, we supplement ~~this~~ these data with several additional near-terminus datasets from the 2013 field campaign (Fig S1), which allows for a detailed bathymetry map along the grounding line. The new data consists of circa 39,000 depth readings taken with Jetyak-mounted (Kimball et al., 2014) and ship-mounted ADCPs. In addition, there are approximately 6000 readings from ~~the~~ a ship-mounted ~~NMEA~~ National Marine Electronics Association (NMEA) bottom-range profiler and 6 readings from ~~XCTDs~~ Expendable CTD sensors (XCTDs) deployed in the otherwise undersampled region of the main plume. Most of these readings are ~~between~~ within 10–100 m ~~from~~ of the glacier front.

Fig 1c shows the new bathymetry at the glacier front as a function of $x$, the distance along the glacier front. The bathymetry can be split into two main regimes: For $x < 1800$ m (the promontory) the glacier is grounded in shallow waters and its surface heights are elevated substantially above flotation. From here on, we refer to the eastern part of the glacier ($x > 1800$ m) as the ~~'main'~~ "main" glacier. In 2013, the front of the promontory was grounded on a sill that runs parallel to the glacier front. This sill coincides approximately with the furthest advance of the glacier in 1992 (Stevens et al., 2016). By 2013 the main glacier had retreated ~ 500 m from the sill, but the promontory was still perched on it in bathymetry of 60 m depth or less (Fig 1c). Since 2013, this part of the glacier front has also retreated by several hundred meters (Fig S2). In 2013, the main part of the glacier front was in waters of depth ~~40-150~~ 40 – 150 m. A pronounced dip in bathymetry – suggestive of a subglacial channel – is found near the location of the main plume ($x = 2000 - 2400$ m). A number of smaller dips are observed between $x = 3400 - 4700$ m. Beyond ~~4700~~ 4700 m the water depth decreases as one approaches the northeastern shoreline.

### 2.2 Glacier surface topography

We obtained a digital elevation map (DEM) from an ArcticDEM overflight on 22 March 2013, which covers the full span of the Saqqarliup glacier front and some of the upstream region (Fig 1). The DEM has a horizontal resolution of 2 m and is capable of resolving individual crevasses on the glacier surface.

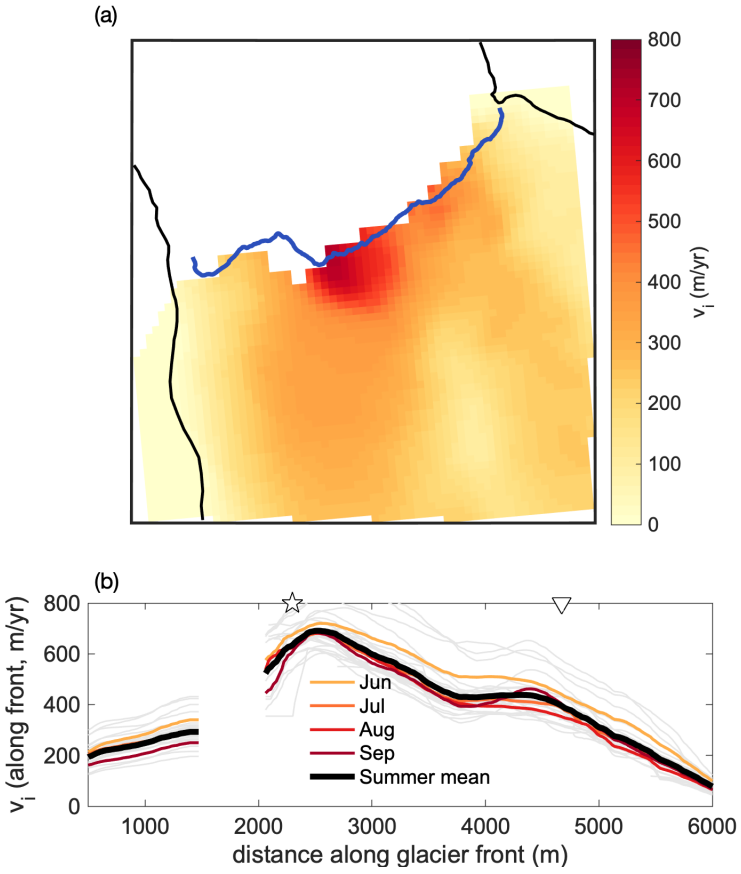


**Figure 2.** (a) InSAR ~~Ice~~ ice velocity data near the glacier front. Shown are mean summer (June–September) values averaged over 28 velocity fields, collected during 2012–2014. Note that there is a consistent data gap near the promontory. The shading represents the horizontal velocity magnitude. (b) Velocity profiles along the glacier front. Here, as in all figures, the ~~perspective~~ orientation is ~~with the direction of ice flux into the page~~looking down-glacier. The faint gray lines show the 28 individual velocity fields. Also indicated are the approximate locations of the two plumes (☆, ▽).

The DEM shows that the front of the glacier is heavily crevassed and has several pronounced dips in the surface elevation at the terminus. The ice cliff is highest (up to 50 m) and most uniform in the region of the promontory, while the main part of the glacier is much more variable with four distinct depressions that reach below 10 m surface elevation (indicated by symbols in Fig 1).

The coincident high-resolution surface elevation and bathymetry data near the terminus enables us to compute the total ice thickness along the glacier front ~~, $H(x)$,~~ which allows for an estimation of the total ice flux (discussed in Section 3.1).

~~The data suggests that the terminus might be floating at several locations: the four highlighted surface depressions at the glacier front are all low enough to raise the isostatic bottom of the ice above the local sea floor.The locally-isostatic bottom of the ice is indicated in Fig 1c (blue dashed line~~

## 3 Components of the frontal mass balance

In order for the mass budget along the glacier front to be balanced, the sum of advective ice flux and frontal retreat must be balanced by total ablation (i.e., by the sum of melting and calving fluxes). Here we ~~assume an average ice density of 883 kg m$^{-3}$, obtained as a mean of low and high values commonly used for glacier and ice shelf front densities, namely 850 kg m$^{-3}$ (Silva et al., 2006) and 917 kg m$^{-3}$ (pure ice). It should be noted that the surrounding ice and the associated stiffness of the glacier will likely prevent the ice from assuming local isostasy everywhere~~ consider a steady state, vertically averaged balance. At a given point $x$ along the glacier front ~~. However, the isostatic bottom can be used to compute a lower bound on~~ this can be written as

$$H\,(R + v_i) = D\bar{M} + C. \tag{1}$$

The left hand side represents retreat and advection, where $H$ is the ice thickness (in m), $R$ is the retreat rate, and $v_i$ the ice velocity at the terminus (both in m yr$^{-1}$). The first term on the right represents the ice loss due to submarine melting, where $D$ is the draft of the glacier (in ~~regions where the ice may be floating. It may be speculated that the ice appears to be floating in these regions due to undercutting by submarine melt (which in turn is associated with rising discharge plumes, as discussed in Section 3.1). The ice would be grounded everywhere else. In particular, the ice surface is elevated substantially beyond its isostatic height in~~ m) and $\bar{M}$ is the ~~region of the promontory.~~ depth-averaged melt rate (in m yr$^{-1}$). The final term, $C$, is the volume loss due to calving (in m$^2$ yr$^{-1}$). In this section we discuss the data used and assumptions made to estimate each term in detail.

~~(a) Mean July ice velocity along the glacier front in blue (right vertical axis). Here we used cubic interpolation to fill the data gap shown in Fig 2. In blue (right vertical axis) is shown the estimated ice thickness along the glacier front, obtained by computing the difference of the surface and bathymetry profiles of Fig 1(c). The dotted red line shows the ice thickness at the glacier front assuming the ice is locally in isostatic equilibrium everywhere. (b) Ice flux along the glacier front (in black), computed from the product of velocity and thickness (shown in panel a). The shaded gray areas under the curve show the ice-flux range due to potential flotation. This is a result of the thickness ranges indicated as red shaded areas in panel a. Also indicated are the approximate locations of the two known plumes (☆, ▽), which coincide with two areas of possible flotation.~~

~~Seasonal advance and retreat of glacier front. (a) 15 front profiles acquired from February to September 2013; the legend highlights every 2nd profile. The thick red and blue profiles represent the May–June and Sept averages, respectively. Also indicated are the location of the two plumes (☆, ▽). (b) Mean front position, shown as an anomaly from the yearly mean position. 2012 values are shown in gray, 2013 in black. The spring profiles used in panel (a) are highlighted in red, fall profiles~~

~~in blue. The vertical dotted lines demarcate the period from 12 to 31 July during which calving was observed. (c) Retreat rates, $R(x)$, along the glacier front. The dashed line represents the spring–fall mean retreat rates; the solid line that of 9 to 31 July, computed from the profiles marked green in panel (b).~~

## 4 ~~Ice flux and retreat~~

### 3.1 Ice velocity and advective ice flux

### 3.2 ~~Ice velocity and advective ice flux~~

Several dozen ice-velocity reconstructions of the lower part of the glacier are available for the years 2009 – 2015 from InSAR data (Joughin et al., 2011). The mean flow velocity at the glacier front (averaged over all available fields) is ~ 350 m yr$^{-1}$ with minima at the edges of the glacier. There is a notable peak in ice velocity (up to ~~750~~ 750 m yr$^{-1}$) near the location of the main plume (Fig 2). A second region of elevated velocities is found near $x = 4500$ m and is more pronounced further upstream from the glacier front. The drainage location of this second ice stream coincides with that of the secondary plume. It is worth noting that the spatial distribution of velocities was remarkably consistent during summer months (June–September) from 2012–2014 (Fig 2b), followed by a substantial overall slowdown in ~~2015 (not shown). This slowdown~~ 2015. This slowdown is not included here as it has been linked to a major drainage event of lake Tininnilik (Kjeldsen et al., 2017), and therefore is subject to altogether different environmental forcing. In what follows, we will consider the 2012–2014 mean July velocity profile along the glacier front. Using the mean summer (May–September) velocities instead does not change the results appreciably.

The magnitude of the summer ice velocity along the glacier front, $v_i(x)$, shown in Fig 2b, together with the ice thickness profile $H(x)$, allows for an estimate of total advective ice flux (Fig 3). This assumes plug flow, i.e., that the ice velocity is approximately constant from the surface to the ice–bedrock interface~~, which is~~ . Note that for a glacier with no sliding and uniform temperature, the depth-averaged velocity is 80% of the surface velocity. For fast-flowing tidewater glaciers with concentrated deformation at depth, such as Saqqarliup, plug flow is therefore considered a good approximation ~~for fast-flowing tidewater glaciers (Meier and Post, 1987). The~~ (Meier and Post, 1987).

We note that the thickness data suggest that the terminus might be floating at several locations: the four highlighted surface depressions at the glacier front are all low enough to raise the isostatic bottom of the ice above the local sea floor. The locally-isostatic bottom of the ice is indicated in Fig 1c (blue dashed line). Here we assume an average ice density of 883 kg m$^{-3}$, obtained as a mean of low and high values commonly used for glacier and ice shelf front densities, namely 850 kg m$^{-3}$ (Silva et al., 2006) and 917 kg m$^{-3}$ (pure ice). The surrounding ice and the associated stiffness of the glacier will likely prevent the ice from assuming local isostasy everywhere along the glacier front. However, the isostatic bottom can be used to compute a lower bound on the ice thickness in regions where the ice may be floating. It may be speculated that the ice appears to be floating in these regions due to undercutting by submarine melt (which in turn is associated with rising discharge plumes, as discussed in Section 3.1). The ice would be grounded everywhere else. In particular, the ice surface is elevated substantially beyond its isostatic height in the region of the promontory. The uncertainty in ice thickness associated with the

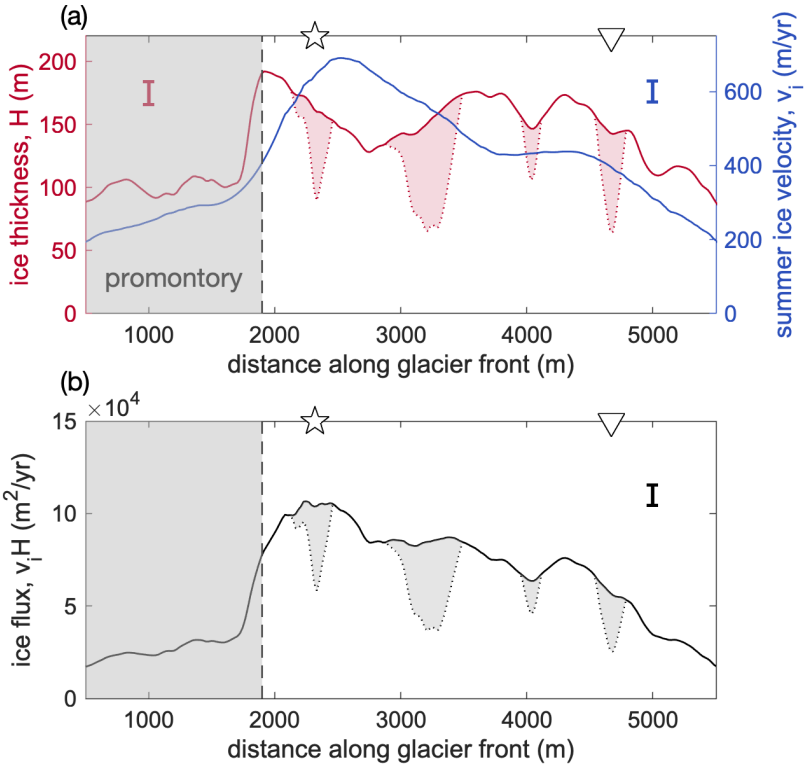


**Figure 3.** (a) Mean July ice velocity along the glacier front in blue (right vertical axis). Here we used cubic interpolation to fill the data gap shown in Fig 2b. In red (left vertical axis) is shown the estimated ice thickness along the glacier front, obtained by computing the difference of the surface and bathymetry profiles of Fig 1c. The dotted red line shows the ice thickness at the glacier front assuming the ice is locally in isostatic equilibrium everywhere. (b) Ice flux per unit width along the glacier front (in black), computed from the product of velocity and thickness (shown in panel a). The shaded gray areas under the curve show the ice-flux range due to potential flotation. This is a result of the thickness ranges indicated as red shaded areas in panel a. Uncertainties for thickness, velocity, and ice flux are shown by the red, blue, and black standard error bars, respectively. Also indicated are the approximate locations of the two known plumes (☆, ▽), which coincide with two areas of possible flotation.

glacier potentially floating at several points ~~along the front~~ is illustrated by the shaded areas in Fig 3. In the figure, the upper bound of the ice thickness assumes a fully grounded glacier front, while the lower (dashed) bound assumes local isostasy everywhere. The ice flux is highest when assuming a fully grounded glacier, while a partially floating glacier front would have a correspondingly reduced flux.

### 3.2 Changes in glacier front position

Superimposed on the aforementioned long-term retreat of the glacier front over the past decades (Fig S2) we observe a seasonal advance–retreat cycle during 2012 and 2013 (Fig 4). A total of 27 front positions between January–October 2012 and January–

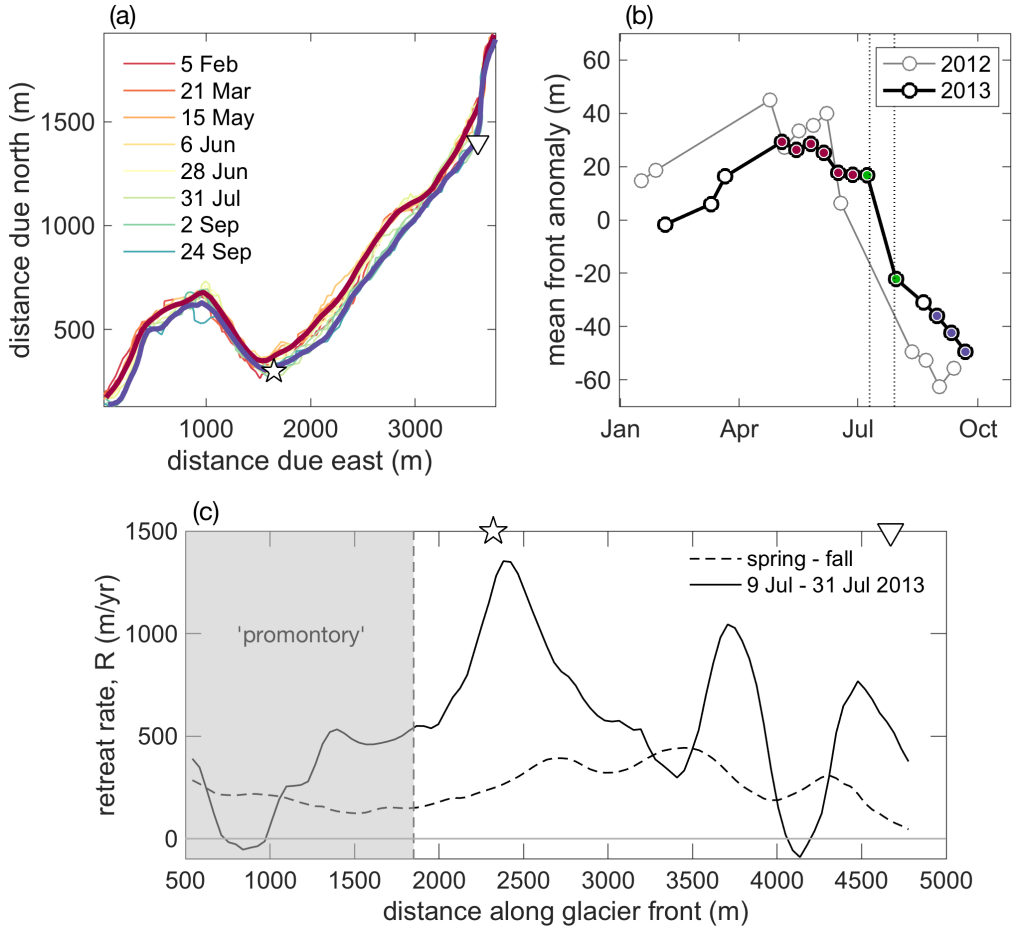


**Figure 4.** Seasonal advance and retreat of glacier front. (a) ~~Close-up of glacier~~ 15 front ~~and adjacent fjord, with~~ profiles acquired from February to September 2013; the legend highlights every 2nd profile. The thick red ~~rectangle outlining~~ and blue profiles represent the ~~region of interest (panel b)~~ May–June and ~~red stars indicating~~ September averages, respectively. Also indicated are the location of the ~~wave moorings;~~ two plumes (b☆, ▽)~~spatial calving distribution as estimated from pressure sensor data; the shaded rectangle indicates the promontory;~~. (~~e~~b) ~~calving count along glacier~~ Mean front position, ~~obtained~~ shown as ~~total number of calving events detected within a 300 m running window along~~ an anomaly from the ~~glacier front~~ yearly mean position. 2012 values are shown in gray, 2013 in black. The spring profiles used in panel (a) are highlighted in red~~bars~~, ~~left axis)~~fall profiles in blue. ~~Also shown is an estimate for~~ The vertical dotted lines demarcate the ~~relative~~ period from 12 to 31 July during which calving ~~volume~~was observed. (c) Retreat rates, ~~computed from~~ $R(x)$, along the ~~product of the frequency of calving events~~ glacier front. Positive $R$ represents glacier retreat and negative $R$ glacier advance. The dashed line represents the ~~corresponding magnitudes of~~ spring–fall 2013 mean retreat rates; the ~~detected waves (black~~ solid line that of 9 to 31 July, ~~right axes). Plume and surface dip locations are indicated as~~ computed from the profiles marked green in ~~previous figures~~panel b.

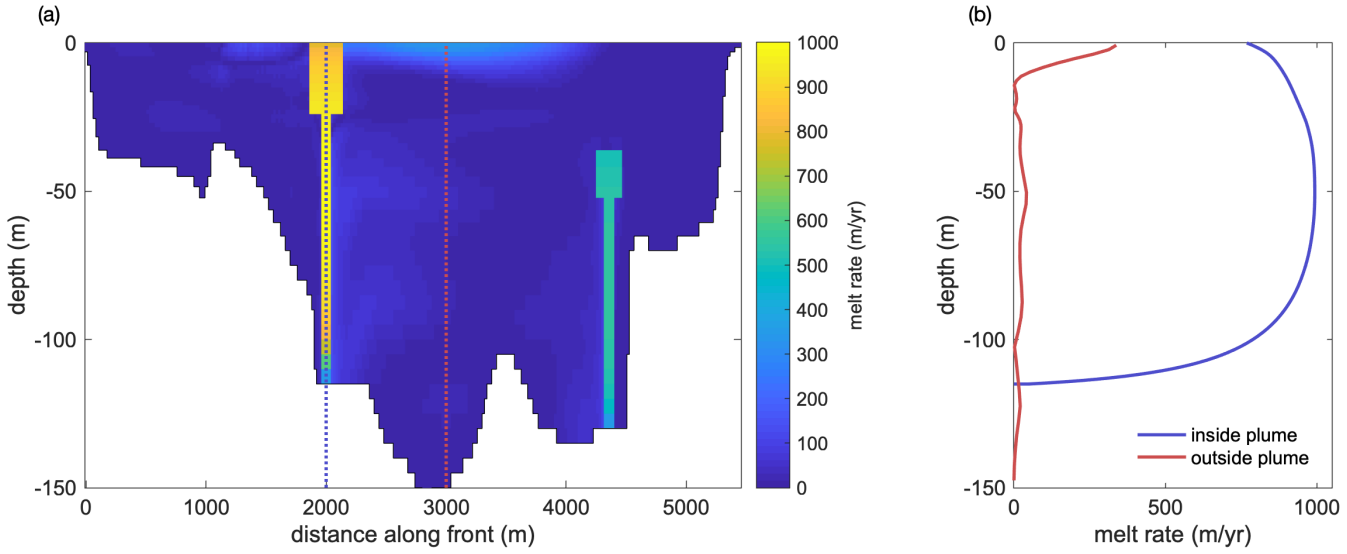


**Figure 5.** (a) Time-mean melt rates along the glacier front as estimated from MITgcm, adapted from Slater et al. (2018), their Fig 3f. The bathymetry in the model (white) is based on that of Stevens et al. (2016). (b) Melt rates averaged inside the main discharge plume (blue) and outside of both plumes (red). The gray area is magnified in panel (c), highlighting the increased melt rates near the surface.

October 2013 were digitized from TerraSAR-X satellite images. The 15 profiles from 2013 are shown in Fig 4a. Both years exhibit a clear, albeit modest, seasonal cycle in terminus ~~migration~~position, with a ~~spatial-mean advance~~ mean advance for the entire front of roughly 30 m from January through April/May, followed by a more rapid retreat from June to September of circa 80 m (Fig 4b). However, there is substantial ~~along-glacier variability~~ variability along the glacier front in this cycle. Near the edges of the glacier, and in particular at the promontory, the glacier exhibits a much reduced advance–retreat cycle, and more variable regions are found in the main dynamic section of the glacier.

~~We define~~ $R(x)$ ~~as the rate of retreat of the glacier front at location $x$, in m yr$^{-1}$. $R(x)$~~ is computed as the rate of retreat perpendicular to the initial glacier front. The most rapid retreat in 2013 was observed at the time of the July study period. Fig 4b shows the spatial-mean seasonal retreat anomalies for 2012 and 2013, with profiles from 9 July and 31 July 2013 highlighted in green. Such rapid retreat is spatially highly variable (Fig 4c) and ~~likely~~ strongly impacted by sporadic but large individual calving events. Longer-term mean retreat rates, computed from average spring and fall glacier front positions (highlighted in Fig 4 in red and blue, respectively) may therefore be more representative on longer time scales.

## 4 ~~Ablation~~

### 3.1 Submarine melting

In order for the mass budget along the glacier front to be balanced, the sum of advective ice flux and frontal retreat must be balanced by total ablation (i. e. , by the sum of melting and calving fluxes). Here we consider a steady state, vertically averaged balance. At a given point $x$ along the glacier front this can be written as

$$H\left(R+v_i\right)=D\bar{M}+C.$$

The terms on the left hand side (retreat rate and advective ice flux) have been discussed in Section 3.1. The first term on the right represents the ice loss due to submarine melting, where $D$ is the draft of the glacier and $\bar{M}$ is the depth-averaged Submarine melt rates at Saqqarliup Sermia during summer 2013 have been estimated by Slater et al. (2018). Here we provide only a brief overview of the approach and build on the results of Slater et al. (2018) to investigate the glacier's flux balance. Melt rates within the two plumes were estimated using standard buoyant plume theory (Jenkins, 2011; Carroll et al., 2016; Slater et al., 2016) . Melt rates outside of the plumes were estimated using a high-resolution numerical model of the fjord in the Massachusetts Institute of Technology general circulation model (MITgcm), which has become the leading model for simulating the circulation and water properties of glacial fjords and for estimating the resulting submarine melt rates (e.g. Xu et al., 2012; Sciascia et al., 2013; Cowto . Both buoyant plume theory and MITgcm were forced with runoff from the regional climate model RACMO and initialized with hydrographic profiles from the fjord. Slater et al. (2018) also presented observationally-inferred melt rates using water property and velocity measurements collected within 100 m of the calving front. In each approach, Slater et al. (2018) then used the standard three-equation melt rate parameterization of Holland and Jenkins (1999) to convert the modeled or observed water properties and velocities to an estimated submarine melt rate. $\bar{M}$ is derived from in-situ hydrographic observations , in concert with a high-resolution numerical model (see Section 3.1). The final term on the right hand side of equation is the volume loss due to calving. This is estimated from in-situ pressure sensors (see Section 3.2), and presents the least well constrained term of equation There is good agreement between the melt rates estimated with MITgcm and with observations (Slater et al., 2018, their Fig 3). Here, we only consider the modeled melt rates (Fig 5), which have the advantage of covering the whole extent of the glacier front (unlike rates inferred from observations, which have data gaps in and around the plumes).

In what follows we consider the volume flux across the glacier front during the summer of 2013. We make the assumption that this flux was steady during the study period and ignore time-dependencies of the individual terms in equation There is large spatial variability in submarine melt rates along the glacier front (Fig 5). Submarine melt rates are highest (both in a depth-averaged and maximum sense) within the two plumes where the discharge of buoyant surface meltwater from beneath the glacier gives high water velocities. Outside of the two plumes melt rates are much smaller in a depth-averaged sense, however the lateral circulation excited by the plumes combines with warm surface waters to give high melt rates near the surface outside of the plumes (Fig 5c; Slater et al., 2018).

While these melt-rate estimates represent the state-of-the-art in terms of melt-rate modeling, we stress that they are based on a melt-rate parameterization that has not been confirmed by observations, especially for the case of a mostly vertical front of a tidewater glacier. The uncertainty associated with these melt-rate estimates is further discussed in Section 5.

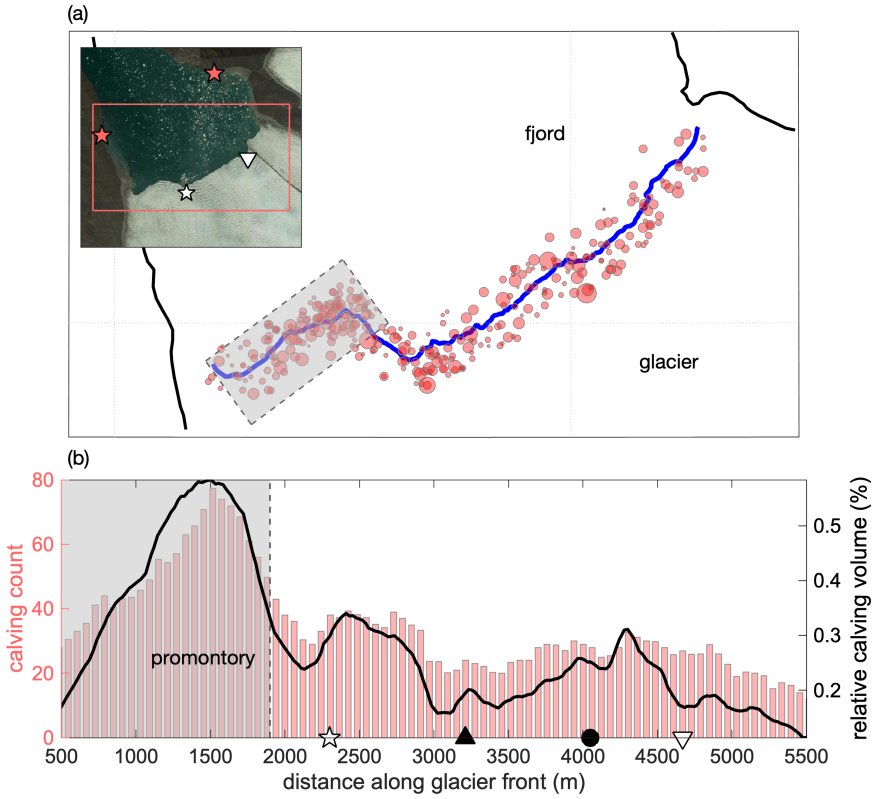


**Figure 6.** (a) Close-up of the glacier front and adjacent fjord, with the red rectangle outlining the region of interest (panel b) and red stars indicating the location of the wave moorings; (b) spatial calving distribution as estimated from pressure sensor data; the shaded rectangle indicates the promontory; (c) calving count along the glacier front, obtained as the total number of calving events detected within a 300 m running window along the glacier front (red bars, left axis). Also shown is an estimate for the relative calving volume, computed from the product of the frequency of calving events and the corresponding magnitudes of the detected waves (black line, right axes). Plume and surface dip locations are indicated as in previous figures.

### 3.2 Calving frequency and distribution

Calving events were detected over a 19-day period from 12 July to 31 July 2013, using two pressure sensor moorings located on the western and eastern banks of the fjord, each at a distance roughly 2 km from the nearest point along the glacier front (Fig 6a). The dispersion of waves that are created by individual calving events can be inverted to estimate the distance between the mooring and the origin of the wave. Wave packets that are detected by both moorings can be used to triangulate the time and position of the corresponding calving event (Minowa et al., 2018). ~~The~~ For the present dataset, this method has been validated against a photography-derived calving record ~~by~~ and good correspondence was observed (not shown). The study by Minowa et al. (2018) provides a detailed description of the method.

In total, 336 calving events were identified using this method over the period that both sensors were recording. Fig 6b shows the location and ~~an estimated magnitude~~ wave amplitude of the individual events. The calving frequency distribution along the glacier front is illustrated in Fig 6c.

A pronounced peak in frequency is found at the promontory, where shallow bathymetry causes the glacier to be elevated substantially beyond its isostatic height of flotation. With its high ice cliffs the promontory can be regarded as a region that is subject to a rather different calving regime than the rest of the glacier.

For the main part of the glacier, we observe a peak in calving activity at a distance $x \approx 2400$ m along the glacier front, near the concave bend in the glacier front (Fig 6b). A second peak in calving activity is found around $x \approx 4300$m. Both peaks appear slightly offset from the location of the two plumes. The calving activity is lowest at the northeast edge of the ~~glacier~~terminus.

Even though this dataset presents a rather accurate record of calving frequencies, it remains challenging to infer a total volume of calved ice (Minowa et al., 2018). This is due to the different modes of calving (e.g., ~~ice cliff~~ ice-cliff calving versus submarine calving), as well as the different shapes of calved ice blocks and the differing heights from which they fall (or depths from which they rise). Distinguishing between these events from the pressure sensor data is a difficult task and beyond the scope of this study. The pressure sensors do record an amplitude of the incoming wave packet associated with a given calving event~~, and assuming~~ . Crudely approximating that this amplitude is ~~correlated with~~ proportional to the size of the calved ice we can estimate a relative calving volume (black curve in Fig 6b). However, since a small cone-shaped ice block can act as a more efficient wave generator than a large flat piece of ice (N. Pizzo, personal communication, Bühler, 2007), it is difficult to ascertain a direct relation between wave amplitudes and calving volume. In what follows we therefore only consider the calving frequency record and will scale this record such that the resulting ~~mean~~ calving flux approximately closes the mass budget at the glacier front (see Section 4.2). Given the limitations of the data, we take such a scaling to be the most justifiable first-order approximation, supported by the rather uniform distribution of estimated calving event sizes along the glacier front.

### 3.3 ~~Submarine melting~~

~~The submarine melting regime at Saqqarliup has been studied in detail by **?** and is briefly described here. Submarine melt rates are thought to respond primarily to fjord water velocities and temperatures adjacent to the calving front (Holland and Jenkins, 1999) . Given the great difficulties of directly measuring submarine melt rates, it is common to instead estimate water velocities and temperatures and then employ a parameterization to estimate melt rates. **?** used both data collected close to the calving front and a numerical model to estimate water properties, and thus, submarine melt rates at Sarqardleq Sermia. There is good agreement between the melt rates estimated with the numerical model and with the observations. Here, we only consider the modeled melt rates, which have the advantage of covering the whole extent of the glacier front(unlike rates inferred from observations, which have data gaps in and around the plumes).~~

~~The most relevant term for the frontal mass budget is~~ The scaling factor is chosen such that the mean calving volume is equal to the ~~depth-averaged melt rate (Fig 7b). However, we also consider the possibility for melting to have a dynamic impact on calving , in which case the vertical profile of the melt rates becomes of interest.~~ mean of the residual, i.e. $\langle C \rangle = \langle H(R + v_i) - D\bar{M} \rangle$.

There is large spatial variability in submarine melt rates along the glacier front. Submarine melt rates are highest (both in a depth-averaged and maximum sense) within the two plumes where the discharge of buoyant surface meltwater from beneath the glacier gives high water velocities. Outside of the two plumes melt rates are much smaller in a depth-averaged sense, however the lateral circulation excited by the plumes combines with warm surface waters to give high melt rates near the surface outside of the plumes (?).

While these melt-rate estimates represent the state-of-the-art in terms of melt-rate modeling, we stress that they are based on a melt-rate parameterization that has not been confirmed by observations, especially for the case of a mostly vertical front of a tidewater glacier.The uncertainty associated with these melt-rate estimates is further discussed in Section 5.

## 4 Overall flux balance and spatial variability

### 4.1 Frontal mass budget

In what follows we consider the volume flux across the glacier front during the summer of 2013. We make the assumption that this flux was steady during the study period and ignore time-dependencies of the individual terms in equation (1).

To compare the different terms in the overall mass budget, we consider the retreat rate as computed from the two fronts measured on 9 and 31 July 2013, since this is almost the exact time window of the calving observations (12 – 31 July). For the advection term we use the July average over the years 2012 – 2014, since the July 2013 ice velocity fields have substantial data gaps at the glacier front. However, as discussed above, there is little interannual variability in $v_i$ over these years, so the 3-year mean likely gives a close approximation to the July 2013 velocity field. Front retreat , advective flux , and their sum and advective flux (i.e., the left hand side of equation 1) are shown in Fig 7a. Melt fluxes, estimated calving volumes, and their sum (i.e., the right hand side of equation 1) are shown The sum of ice advection and retreat is compared to the estimated melt fluxes in Fig 7b. The two sides of equation 1 are compared directly in Fig 7c . shows the calving flux as estimated from the observations, compared to the residual $C$ of the other three terms in equation 1, such that $C = H(R + v_i) - D\bar{M}$.

Integrated along the main part of the glacier front we estimate an ice advection rate of $0.2 \pm 0.05$ Gt yr$^{-1}$ and a retreat rate of $0.3 \pm 0.16$ Gt yr$^{-1}$. The uncertainty in ice advection corresponds to one standard deviation in the spread of mean July ice velocities. The uncertainty in the retreat rate corresponds to one standard deviation in spatial variability between the July 2013 retreat rate and the spring–fall retreat rate. This gives as a best estimate for the total rate of ice loss $\sim 0.5$ Gt yr$^{-1}$.

Using the aforementioned melt-rate parameterizations we find a total melting flux of $0.03$ Gt yr$^{-1}$. This would suggest that $94\%$ ($0.47$ Gt yr$^{-1}$) of ablation occurs in the form of calving. Thus, the glacier would lose mass almost exclusively due to calving in most places, apart from in localized areas near the subglacial discharge plumes. However, there are large uncertainties associated with the total melt-rate estimate. And even for a small total melt flux, melting may be important for the overall flux balance due to its dynamic impact on calving. These findings are discussed further in Section 5.

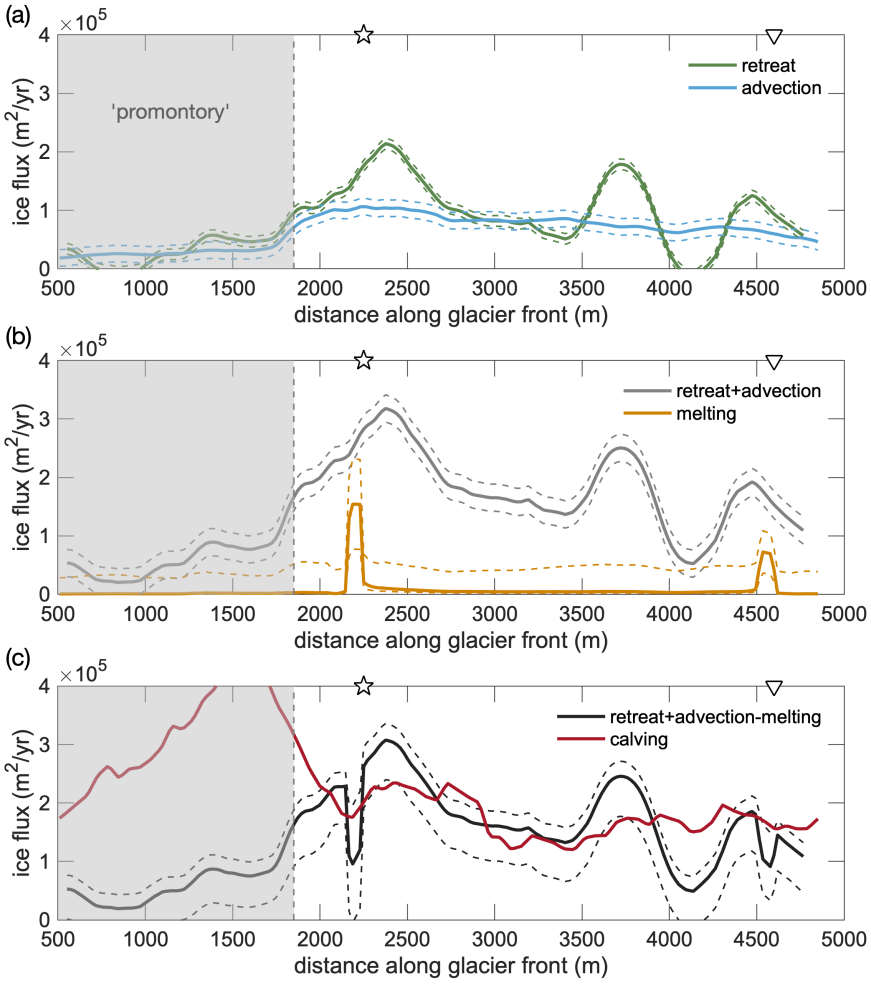


**Figure 7.** Flux balance along the glacier front. Dashed lines indicate uncertainties as discussed in the text. (a) The green line represents the July 2013 retreat rate and the blue line the advective ice flux. ~~The sum of these two terms (black) must be equal to total ablation.~~ (b) ~~Melt flux~~ Sum of retreat and advection (~~red~~gray) and ~~calving~~ melt flux (~~dark red~~orange). ~~The total ablation, i.e., the sum of melting and calving, is shown by the gray line. Note that the calving flux has been scaled to approximately close the budget.~~ (c) Approximate closure of the volume flux budget along the glacier front. The black line shows the ~~sum~~ residual of ~~ice~~ advection ~~and~~ plus retreat ~~as in panel (a)~~minus melting, while the ~~gray~~ red line shows the ~~total ablation~~ observational calving estimate as in panel ~~(~~b~~)~~. Note that the calving flux has been scaled to approximately close the budget for the main part of the glacier.

### 4.1 High spatial variability along the glacier front

A striking feature of almost all components of this multipartite dataset is their high spatial variability along the glacier front.

~~The~~ Away from the margins, the ice thickness at the front ranges from thin (<40 m) sections near the northeast edge to ~100 m along the promontory and up to 192 m near the main plume, with substantial variations throughout. Overall, we observe a mean thickness of 128 m with a variability of ±38 m (one standard deviation).

We find that the advective flux is suppressed at the promontory and highest near the outflow location of the main plume, with a second smaller peak near the secondary plume (Fig 3).

The retreat rates are overall of comparable magnitude to the advective flux. However, the retreat rates are spatially extremely variable, in particular the observed July 2013 rates, which exhibit three regions of enhanced retreat, two of which are close to the two discharge plumes, with peaks at $x$ = 2400 and 4400 m (Fig 4c). Averaged over longer time periods, the retreat rates ~~also~~ become more uniform~~(as discussed above), which suggests that observations~~ , in contrast to those over shorter time periods ~~are~~ which are likely more strongly influenced by individual calving events.

The melting estimates feature two pronounced maxima at the plumes and are small everywhere else (Fig 7b). The maximum melt flux value at the main plume ($1.5 \times 10^5$ m$^2$ yr$^{-1}$) is slightly higher than the mean retreat and advective flux values ($1.0 \times 10^5$ and $0.8 \times 10^5$ m$^2$ yr$^{-1}$, respectively). Outside the two plumes the mean melting flux ($0.04 \times 10^5$ m$^2$ yr$^{-1}$) is an order of magnitude lower than inside the plume and than the other budget terms. Dividing these depth-integrated flux values by the average thickness (128 m), we obtain depth-averaged velocities for each term. These are ice advection: 780 m yr$^{-1}$; retreat: 620 m yr$^{-1}$; maximum melt rate at main plume: 1200 m yr$^{-1}$; and mean melt rate outside the plumes: 30 m yr$^{-1}$.

Calving frequencies are strongly enhanced at the promontory, which – given the reduced advection and retreat in this area – ~~suggests~~ implies that calved pieces are in general smaller here. Since we are unable to adequately distinguish between the different calving sizes, the heightened calving activity at the promontory results in a large discrepancy between the ~~estimated total ablation and the sum of retreat and advection~~ computed residual $C$ and the observationally estimated calving flux in that region (~~gray and black curves in~~ Fig 7c). We may also be underestimating the advective flux at the promontory slightly, since we only consider horizontal velocities, and the ice flow may have a non-negligible vertical component as the glacier rides onto the local sill. Even though calving frequencies are overall lower for the main part of the glacier, we observe two local maxima, slightly offset from the plumes (Fig 7b). Some of the lowest calving frequencies are found between the two plumes in the region farthest from both plumes.

The two peaks in depth-averaged melt flux (Fig 7b), co-located with the two discharge plumes, are just offset from the two peaks in frontal retreat and calving. ~~The maximum melt flux value ($1.5 \times 10^5$ m$^2$~~

### 4.2 Spatially integrated mass budget

Integrated along the main part of the glacier front we estimate an ice advection rate of $0.2 \pm 0.05$ Gt yr$^{-1}$ ~~) is slightly higher than the mean retreat and advective flux values ($1.0 \times 10^5$ and $0.8 \times 10^5$ m$^2$~~ and a retreat rate of $0.3 \pm 0.03$ Gt yr$^{-1}$. This gives as a best estimate for the total rate of ice loss ~ 0.5 Gt yr$^{-1}$. The uncertainty in ice advection corresponds to one standard deviation in the spread of mean July ice velocities. The uncertainty in the retreat rate is largely due to the somewhat arbitrary selection of "before" and "after" dates, and the resultant disproportionate impact of individual calving events. The error reported here is

one standard deviation in the difference in retreat when choosing the frontal profiles of June 28 (instead of July 9) as "before" date or August 22 (instead of July 31) as the "after" date.

Integrating the estimated melt over the main glacier front gives a total melting flux of 0.03 Gt yr$^{-1}$~~, respectively) . Outside the two plumes the mean melting flux ($0.04 \times 10^5$ m$^2$ yr$^{-1}$) is an order of magnitude lower than inside the plume and than the other budget terms.~~. This would suggest that ~ 0.47 Gt yr$^{-1}$ (or 94%) of ablation occurs in the form of calving, thus implying that the glacier balances the ice flux almost exclusively through calving (except in the narrow regions at the discharge plumes). The lack of an ice mélange in the fjord, and the anecdotal observation of limited calving are, however, at odds with this finding. This raises the question whether the melt term – estimated using state-of-the-art parameterizations informed by observations very close to the ice front – is incorrect? This is discussed further in Section 5.

~~In order to approximately balance the total ablation with the sum of ice advection and retreat, we scale the~~ While we have no direct measurement of calving volume, we can close the integrated mass budget by scaling the observed relative calving frequencies ~~by a constant factor. This gives~~ to give the required total calving flux of 0.47 Gt yr$^{-1}$ (Fig 7c). This corresponds to a mean calving flux of $1.7 \times 10^5$ m$^2$ yr$^{-1}$ ~~, which is an order of magnitude larger than the estimated~~ along the glacier front (compared to a mean melting flux of $0.1 \times 10^5$ m$^2$ yr$^{-1}$~~.~~). Again dividing by the average thickness, this corresponds to 1300 m yr$^{-1}$ ice loss due to calving, compared 80 m yr$^{-1}$ of melting.

### 4.3 Variations in the vertical glacier front profile

A final piece of observational evidence which may help in the interpretation of the results above is provided by point cloud images of the glacier front profile. These were collected during the 2013 field season using an autonomous surface vehicle – the Woods Hole Oceanographic Insitution ~~“~~"Jetyak" (Kimball et al., 2014; Mankoff et al., 2016). Among other instruments, the Jetyak carried a multibeam sonar that was mounted sideways facing the glacier, which collected three-dimensional maps of the underwater portion of the glacier front. Further details of the Jetyak's operation and data can be found in Kimball et al. (2014). Here, we highlight several characteristic frontal profiles. Fig 8 shows a point-cloud transect of the northeastern flank of the glacier, as well as four vertical line profiles at different locations along the transect.

The first two profiles (A and B) are placed near the secondary plume. Both profiles are marked by two features: (i) a sloped upper 20–25 m, which results in the above-water cliff of the glacier being set back by 10–20 m, relative to the most ocean-ward point of the glacier face. (ii) Below 40 m depth we observe up to 10 m of undercutting, such that the protrusion beyond the above-water cliff is most pronounced at depths 20–40 m, and the ice is substantially eroded at greater depths. This is likely caused by the rising subglacial plume which leads to preferential melt of the deeper parts of the glacier front (Fried et al., 2015; Slater et al., 2017). Note that the high turbidity of water within the main plume prevented the Jetyak from surveying the shape of the glacier front occupied by that plume.

Profiles C and D, which are located far from the plume, also feature said underwater ice protrusion, however, they show no signs of undercutting. The presence of such net-buoyant underwater protrusions and their potential impact on calving has been studied previously (Wagner et al., 2014, 2016), and will be discussed further in the next section.

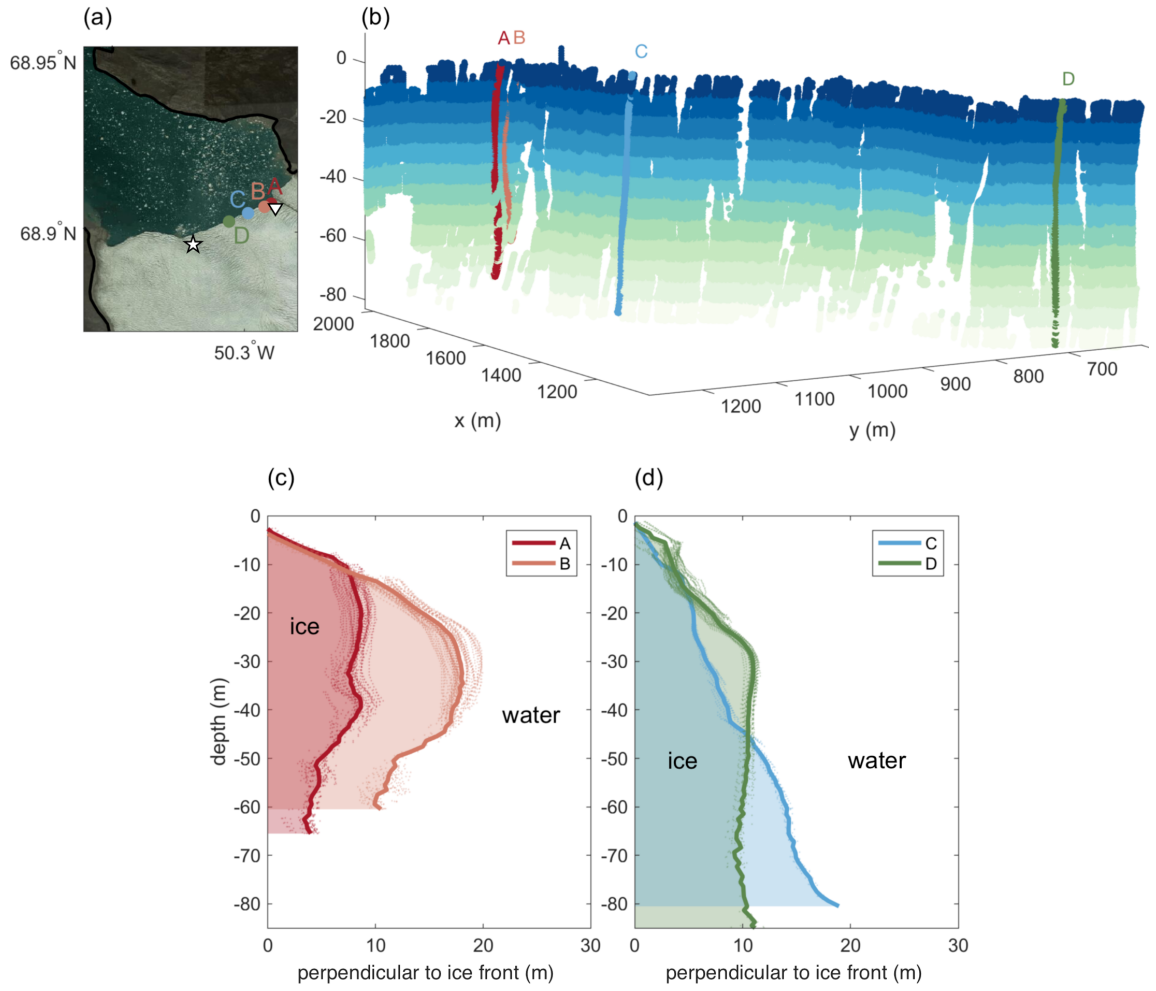


**Figure 8.** Multibeam sonar data of glacier front from 26 July 2013. (a) Map illustrating the location of the shown multibeam cross-sections A–D and the two plumes (☆, ▽). (b) 3D point-cloud transect showing a part of the eastern side of the glacier (distance along glacier front, ~ 4000 – 4800 m). Data is color-coded by depth below sea level. Indicated are the locations of the four cross-sections A–D shown in panels c and d. (c) Cross-sections A and B near subglacial plume, exhibiting characteristic undercutting. (d) Cross-sections C and D away from plume, showing submarine protrusions without undercutting.

We note that the bathymetry reaches depths of around 130 m for this part of the glacier and the bottom ~ 50 m ~~or so~~ are unfortunately not captured by the multibeam sonar. However, the profiles located near the melt (A and B) can be expected to be further undercut below the observed range (Fried et al., 2015), while profiles C and D likely do not feature such undercutting.

## 5 ~~Discussion - the~~ The role of melting in the frontal mass budget

### 5.1 Uncertainty in melt rate estimates

The finding that calving appears to make up almost the entire loss of ice is somewhat unexpected, in particular since during the study period the glacier's calving activity was limited to relatively small events, and the fjord was by-and-large devoid of icebergs.

~~These observations, along with the large uncertainty of the melt-rate parameterization used to convert near-ice ocean properties to melt rates , warrants the consideration of an end-member scenario: suppose that submarine melting accounted for all of~~ Furthermore, the ~~frontal ablation beneath the fjord surface , with calving only removing ice above the water. How would the~~ melt rates used here are roughly double that of what previous estimates would have been since we account for additional melt that arises from the recirculation of warm ambient surface waters (Slater et al., 2018). Yet, melting supposedly only makes up ~ 6% of the total ablation.

Given the lack of observational verification of the current melt rate parameterization~~need to be modified in order to achieve this? Scaling the turbulent transfer coefficients~~ , it is worth considering end-member melt rate scenarios. Perhaps the key parameter in the melt rate parameterization ~~upward by an order of magnitude would increase melt rates by approximately an order of magnitude, allowing the melting outside of~~ is the thermal Stanton number, which directly controls the rate of transfer of heat from the ocean to the ~~plumes to roughly balance the total loss (Figs 7b and c). We do not think this is realistic however as the melt rates inside the plumes would also increase by an order of magnitude,and this would presumably drive retreat at a much faster rate than observed~~ice. Its canonical value is based largely on field observations at a cold Antarctic ice shelf and there are as yet no strong observational constraints from tidewater glaciers. Furthermore, Ezhova et al. (2018) have recently argued for a larger Stanton number based on direct numerical simulations. We thus consider lower and upper bounds for melt rates in which the thermal Stanton number is respectively reduced and increased by 50% (Fig 7b,c).

~~We next consider how water velocity~~ To obtain the upper bound melt rate scenario, we also increase the outside-of-plume water velocity which enters the melt rate parameterization. ~~Since plumes drive an entrainment velocity which is ~10% that of the plume velocity (Morton et al., 1956), mean flow velocities outside of plumes will always be approximately an order of magnitude smaller than inside the plumes. One~~ While vertical velocities inside of plumes might be considered reliable based on well-validated plume theory (Morton et al., 1956), one could argue that the mean modeled ~~velocities, particularly outside the plumes, are~~ outside-of-plume velocities may be too small for a number of reasons including coarse model resolution and the lack of tides, surface waves, and calving events which may excite water motion. These factors might crudely be taken into account by placing an additional velocity in the melt-rate parameterization. Such an approach has some precedent with the inclusion of tides beneath ice shelves (Jenkins and Nicholls, 2010). In ~~order for melting to account for all of the ice loss an additional velocity with magnitude 1~~ the upper bound melt rate scenario, we thus add 0.2 m $s^{-1}$ ~~would have to be added to the parameterization. This appears physically improbable, and perhaps 0.2 m $s^{-1}$ (accounting for ~20% of~~ to the ~~ice loss ) is more reasonable~~outside-of-plume water velocity entering the melt rate parameterization.

In the lower bound melt rate scenario, melting accounts for an even smaller fraction of mass loss than in our best estimate, but is still significant inside the plumes. In the upper bound melt rate estimate, melting accounts for a significant proportion of mass loss both inside and outside of the plumes (Fig 7b). Clearly this is an observationally ~~underconstrained discussion. However, it appears worth highlighting that through a~~ under-constrained discussion, and we emphasize that these upper and lower bounds are very rough error estimates as the state of understanding of submarine melting does not yet permit rigorous quantitative assessment of uncertainties. Yet these bounds do show that through reasonable modification of the melt rate parameterization, melting can account for a larger fraction of the ice loss than reported ~~here.~~

### 5.2 ~~Dynamic impact of melting on overall ablation~~

~~Even if the volume of ice lost through submarine melting is small, melting may still play an important role in the glacier's frontal flux balance: since it is highly focused on discrete regions of~~ in our best estimate. Even by introducing these uncertainties, however, the analysis presented still indicates that calving is the dominant mode of mass loss for most of the glacier front ~~, melting~~ (except at the localized melt plumes).

### 5.2 Impact of melting on calving

In addition to balancing the frontal ice flux, the data allow us examine how melting and calving may be interlinked. Specifically, one consequence of melting being focused on narrow regions is that it can lead to sharp incisions in the ~~front profile that may be significant drivers of~~ glacier front, which in turn may enhance calving.

~~? found that fjord recirculation driven by subglacial discharge plumes can cause substantial near-surface horizontal melting along the glacier front (away from the discharge locations of the plumes~~Slater et al. (2018) found that fjord-scale circulations driven by plumes can result in enhanced submarine melting near the fjord surface in regions distant from the plume Fig 5c). This near-surface melting has in turn been suggested as a potential driver for large calving events at glacier fronts that are floating or close to floating (Wagner et al., 2016): Preferential near-surface melting at the glacier front leads to a horizontal melt incision near the water surface which in turn causes erosion of the above-water ice cliff. As a result, the front of the glacier is left with an underwater protrusion (or ~~"~~"ice foot") as in the profiles C and D of Fig 8. This frontal profile is statically unstable, since the ice foot is net buoyant and exerts bending stresses on the glacier (Robertson et al., 2012; Benn et al., 2017) . Calving events occur when such stresses surpass the yield strength of the terminus. ~~This process has also been observed on icebergs in temperate waters (Scambos et al., 2005; Wagner et al., 2014).~~ It is likely that profiles C and D represent sizable ice feet which exert bending stresses that enhance the calving flux in this region.

Furthermore, it is possible that the regions adjacent to the meltwater plumes are more prone to calving since the high melt rates at the plumes cause vertical incisions in the glacier front (Fried et al., 2015). These in turn would reduce the transverse (i.e., along-front) stability of the terminus, and trigger further calving. A surface expression of such a vertical incision in the glacier front can be found near the main plume in the profile of August 2012 (Fig S2). Considering the particular geometry of Saqqarliup, as the two main plumes drive rapid melt near the two edges of the main part of the glacier, this may cause the

entire front between the plumes to be more prone to calving, in particular since we have found this region to be close to (or at) flotation.

In summary, from the observations presented in the previous sections, we propose that there are two distinct regimes driving ablation at Saqqarliup: (a) melting-dominated ablation in spatially confined regions near the discharge plumes, and (b) calving-dominated ablation in the regions away from the plumes (which may ~~nevertheless~~ be enhanced by near-surface horizontal melt incisions). This is further supported by the local minima in calving activity at the location of the two discharge plumes (Fig 7b). The two ablation regimes are summarized in the schematic of Fig 9.

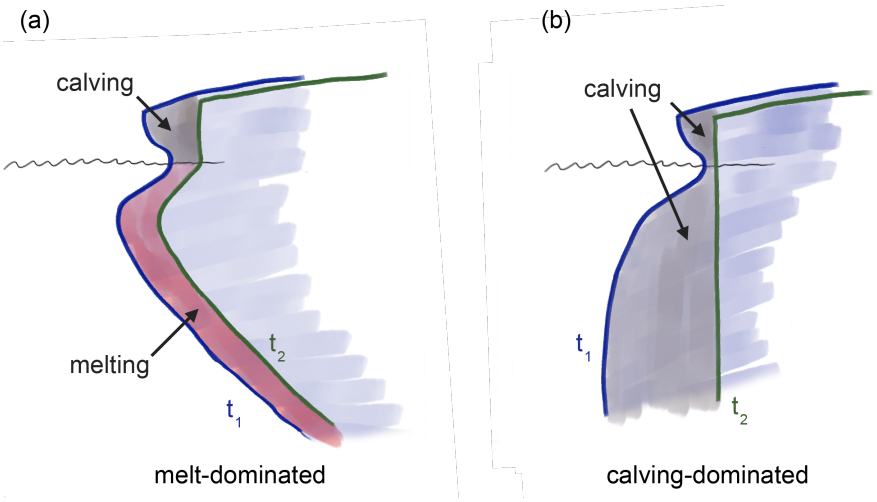


**Figure 9.** Schematics of two distinct ablation regimes. (a) Melt-dominated regime: the vertical structure of melting due to a rising subglacial discharge plume which entrains warm ambient water results in substantial undercutting of the glacier front (as in profiles A and B in Fig 8). These front profiles likely do not cause large calving events with calving mostly confined to the smaller above-water cliff. Profiles are drawn for an earlier time $t_1$ and a later time $t_2$ by which the glacier has retreated mostly due to melting. (b) Calving–dominated regime: here the growth of sizable and buoyant underwater feet (as in profiles C and D in Fig 8) can accelerate calving, with the melt contribution confined to a small region near the water surface. Again, profiles are shown at $t_1$ and $t_2$ (pre and post-calving), as part of the ~~“~~"footloose" calving cycle (Wagner et al., 2014).

## 6 Conclusions

We have presented a multi-faceted dataset of a Greenland tidewater glacier and its surroundings. The unique dataset enables us to investigate the individual terms that determine the flux balance along the glacier front.

We find that the individual terms that comprise the glacier's frontal mass budget are marked by high spatial variability. Ice velocities feature maxima that coincide with troughs in the bathymetry and locations of subglacial discharge plumes. The retreat rates are spatially particularly variable when calculated over shorter periods of time (days to weeks) ~~. Spikes and troughs~~

~~in glacier retreat rates over such short timescales~~ and are likely dominated by somewhat stochastic calving events over such short timescales.

Estimated submarine melt rates from numerical modeling of fjord circulation show rapid melting within the two discharge plumes and more widely at the fjord surface, but limited melting elsewhere. If we use the inferred melt rate to scale the calving flux we find that 94% of the mass balance of this glacier must be balanced by calving. This finding appears to be at odds with the observation of limited calving and the lack of icebergs in the fjord. We suggest that the numerical model – even though constrained by direct measurements and using the standard melt parameterization – may underestimate melting outside of the plumes, indicating that current melt models for tidewater glacier fronts may need to be reviewed and should be treated with caution. ~~Melting, on the other hand, is more consistent throughout the summer and can be expected to only feature gradual changes. Overall, ice loss due to melting , as calculated from commonly used melt-rate parameterizations and observed ocean properties, is an order of magnitude smaller than ice loss due to calving. We note, however, the large uncertainty in the melt rate estimates and stress the possibility that melting could account for a larger proportion of mass loss with modest modifications of the submarine melt rate parameterization .~~

The spatial variability of the observed processes suggests the presence of two distinct ablation regimes: a melting-dominated ~~one~~ regime near the discharge plumes and a calving-dominated regime away from the plumes. We suggest that melting, through its horizontal and vertical variability, may play an important role in driving calving, thus having a dynamic effect out of proportion to the fraction of mass lost by melting. If calving is indeed dependent on the localized melt rates, this may have far-reaching implications for the overall stability of the glacier. Understanding the impact of these spatially highly variable processes on ice sheet dynamics should thus be a priority in the study of ice–ocean interactions.

*Competing interests.* The authors declare no competing financial interests.

*Acknowledgements.* We acknowledge support from the Woods Hole Oceanographic Institution Ocean and Climate Change Institute Arctic Research Initiative, and ~~PLR-1418256~~NSF OPP-1418256 and OPP-1743693, to F. Straneo and S. B. Das. T. J. W. Wagner was further supported by NSF OPP award 1744835. Geospatial support for this work provided by the Polar Geospatial Center under NSF OPP awards 1043681 and 1559691. DEMs provided by the Polar Geospatial Center under NSF OPP awards 1043681, 1559691 and 1542736. D. A. Slater acknowledges the support of Scottish Alliance for Geoscience, Environment and Society early-career research exchange funding.'

## References


Åström, J. A., Vallot, D., Schäfer, M., Welty, E. Z., O'Neel, S., Bartholomaus, T. C., Liu, Y., Riikilä, T. I., Zwinger, T., Timonen, J., and Moore, J. C.: Termini of calving glaciers as self-organized critical systems, Nature Geoscience, 7, 874–878, 2014.

Benn, D. I., Warren, C. R., and Mottram, R. H.: Calving processes and the dynamics of calving glaciers, Earth-Science Reviews, 82, 143–179, 2007.

Benn, D. I., Cowton, T., Todd, J., and Luckman, A.: Glacier Calving in Greenland, Current Climate Change Reports, 3, 282–290, 2017.

Bühler, O.: Impulsive fluid forcing and water strider locomotion, Journal of Fluid Mechanics, 573, 211–236, 2007.

Carr, J. R., Stokes, C. R., and Vieli, A.: Threefold increase in marine-terminating outlet glacier retreat rates across the Atlantic Arctic: 1992–2010, Annals of Glaciology, Vol 27, 1998, 58, 72–91, 2017.

Carroll, D., Sutherland, D. A., Shroyer, E. L., Nash, J. D., Catania, G. A., and Stearns, L. A.: Modeling turbulent subglacial meltwater plumes: implications for fjord-scale buoyancy-driven circulation, Journal of Physical Oceanography, 45, 2169–2185, https://doi.org/10.1175/JPO-D-15-0033.1, 2015.

Carroll, D., Sutherland, D. A., Hudson, B., Moon, T., Catania, G. A., Shroyer, E. L., Nash, J. D., Bartholomaus, T. C., Felikson, D., Stearns, L. A., Noel, B. P. Y., and van den Broeke, M. R.: The impact of glacier geometry on meltwater plume structure and submarine melt in Greenland fjords, Geophysical Research Letters, 43, 9739–9748, https://doi.org/10.1002/2016GL070170, 2016.

Cowton, T., Slater, D., Sole, A., Goldberg, D., and Nienow, P.: Modeling the impact of glacial runoff on fjord circulation and submarine melt rate using a new subgrid-scale parameterization for glacial plumes, Journal of Geophysical Research: Oceans, 120, 796–812, https://doi.org/10.1002/2014JC010324, 2015.

Ezhova, E., Cenedese, C., and Brandt, L.: Dynamics of Three-Dimensional Turbulent Wall Plumes and Implications for Estimates of Submarine Glacier Melting, Journal of Physical Oceanography, 48, 1941–1950, 2018.

Fried, M. J., Catania, G. A., Bartholomaus, T. C., Duncan, D., Davis, M., Stearns, L. A., Nash, J., Shroyer, E., and Sutherland, D.: Distributed subglacial discharge drives significant submarine melt at a Greenland tidewater glacier, Geophysical Research Letters, pp. 9328–9336, 2015.

Hill, E. A., Carr, J. R., and Stokes, C. R.: A review of recent changes in major marine-terminating outlet glaciers in northern greenland, Frontiers in Earth Science, 4, 111, 2017.

Holland, D. M. and Jenkins, A.: Modeling thermodynamic ice-ocean interactions at the base of an ice shelf, Journal of Physical Oceanography, 29, 1787–1800, 1999.

Holland, D. M., Thomas, R. H., De Young, B., Ribergaard, M. H., and Lyberth, B.: Acceleration of Jakobshavn Isbrae triggered by warm subsurface ocean waters, Nature Geoscience, 1, 659–664, 2008.

Howat, I. M., Joughin, I., and Scambos, T. A.: Rapid changes in ice discharge from Greenland outlet glaciers, Science, 315, 1559–1561, 2007.

Howat, I. M., Joughin, I., Fahnestock, M., Smith, B. E., and Scambos, T. A.: Synchronous retreat and acceleration of southeast Greenland outlet glaciers 2000-06: ice dynamics and coupling to climate, Journal of Glaciology, 54, 646–660, 2008.

Jackson, R. H. and Straneo, F.: Heat, salt, and freshwater budgets for a glacial fjord in Greenland, Journal of Physical Oceanography, 46, 2735–2768, 2016.

Jenkins, A.: Convection-Driven Melting near the Grounding Lines of Ice Shelves and Tidewater Glaciers, Journal of Physical Oceanography, 41, 2279–2294, https://doi.org/10.1175/JPO-D-11-03.1, 2011.

Jenkins, A. and Nicholls, K.: Observation and parameterization of ablation at the base of Ronne Ice Shelf, Antarctica, Journal of Physical Oceanography, 40, 2298–2313, 2010.

Jensen, T. S., Box, J. E., and Hvidberg, C. S.: A sensitivity study of annual area change for Greenland ice sheet marine terminating outlet glaciers: 1999–2013, Journal of Glaciology, 62, 72–81, 2016.

Joughin, I., Howat, I. M., Smith, B., and Scambos, T.: MEaSUREs Greenland Ice Velocity: Selected Glacier Site Velocity Maps from InSAR, Version 1, 2011.

Joughin, I., Alley, R. B., and Holland, D. M.: Ice-Sheet Response to Oceanic Forcing, Science, 338, 1172–1176, 2012.

Kimball, P., Bailey, J., Das, S., Geyer, R., Harrison, T., Kunz, C., Manganini, K., Mankoff, K., Samuelson, K., Sayre-McCord, T., Straneo, F., Traykovski, P., and Singh, H.: The WHOI Jetyak: An autonomous surface vehicle for oceanographic research in shallow or dangerous waters, in: 2014 IEEE/OES Autonomous Underwater Vehicles (AUV), pp. 1–7, IEEE, 2014.

Kjeldsen, K. K., Khan, S. A., Bjørk, A. A., Nielsen, K., and Mouginot, J.: Ice-dammed lake drainage in west Greenland: Drainage pattern and implications on ice flow and bedrock motion, Geophysical Research Letters, 44, 7320–7327, 2017.

Luckman, A., Benn, D. I., Cottier, F., Bevan, S., Nilsen, F., and Inall, M.: Calving rates at tidewater glaciers vary strongly with ocean temperature, Nature Communications, 6, 8566, 2015.

Mankoff, K. D., Straneo, F., Cenedese, C., Das, S. B., Richards, C. G., and Singh, H.: Structure and dynamics of a subglacial discharge plume in a Greenlandic fjord, Journal of Geophysical Research: Oceans, 121, 8670–8688, 2016.

Meier, M. F. and Post, A.: Fast tidewater glaciers, Journal of Geophysical Research: Atmospheres, 92, 9051–9058, 1987.

Minowa, M., Podolskiy, E. A., Sugiyama, S., Sakakibara, D., and Skvarca, P.: Glacier calving observed with time-lapse imagery and tsunami waves at Glaciar Perito Moreno, Patagonia, Journal of Glaciology, 21, 1–15, 2018.

Moon, T., Joughin, I., Smith, B., and Howat, I.: 21st-Century Evolution of Greenland Outlet Glacier Velocities, Science, 336, 576–578, 2012.

Morton, B. R., Sir Geoffrey Taylor, F. R. S., and Turner, J. S.: Turbulent gravitational convection from maintained and instantaneous sources, Proc. R. Soc. Lond. A, 234, 1–23, 1956.

Nick, F. M., Vieli, A., Howat, I. M., and Joughin, I.: Large-scale changes in Greenland outlet glacier dynamics triggered at the terminus, Nature Geoscience, 2, 110–114, 2009.

Nick, F. M., Vieli, A., Andersen, M. L., Joughin, I., Payne, A., Edwards, T. L., Pattyn, F., and van de Wal, R. S. W.: Future sea-level rise from Greenland's main outlet glaciers in a warming climate, Nature, 497, 235–238, 2013.

Rignot, E. and Thomas, R. H.: Mass balance of polar ice sheets, Science, 297, 1502–1506, 2002.

Rignot, E., Xu, Y., Menemenlis, D., Mouginot, J., Scheuchl, B., Li, X., Morlighem, M., Seroussi, H., van den Broeke, M., Fenty, I., Cai, C., An, L., and de Fleurian, B.: Modeling of ocean-induced ice melt rates of five west Greenland glaciers over the past two decades, Geophysical Research Letters, 43, 6374–6382, 2016.

Robertson, C. M., Benn, D. I., Brook, M. S., Fuller, I. C., and Holt, K. A.: Subaqueous calving margin morphology at Mueller, Hooker and Tasman glaciers in Aoraki/Mount Cook National Park, New Zealand, Journal of Glaciology, 58, 1037–1046, 2012.

Scambos, T., Sergienko, O., Sargent, A., MacAyeal, D., and Fastook, J.: ICESat profiles of tabular iceberg margins and iceberg breakup at low latitudes, Geophysical Research Letters, 32, 2005.

Sciascia, R., Straneo, F., Cenedese, C., and Heimbach, P.: Seasonal variability of submarine melt rate and circulation in an East Greenland fjord, Journal of Geophysical Research: Oceans, 118, 2492–2506, https://doi.org/10.1002/jgrc.20142, 2013.

Silva, T. A. M., Bigg, G. R., and Nicholls, K. W.: Contribution of giant icebergs to the Southern Ocean freshwater flux, Journal of Geophysical Research: Atmospheres, 111, 2006.

Slater, D., Straneo, F., Das, S. B., Richards, C. G., Wagner, T. J. W., and Nienow, P. W.: Three-dimensional fjord circulation doubles ocean melting of a Greenland tidewater glacier, Geophysical Research Letters, 10.1029/2018GL080763, 2018.

Slater, D. A., Goldberg, D. N., Nienow, P. W., and Cowton, T. R.: Scalings for submarine melting at tidewater glaciers from buoyant plume theory, Journal of Physical Oceanography, 46, 1839–1855, https://doi.org/10.1175/JPO-D-15-0132.1, 2016.

Slater, D. A., Nienow, P. W., Goldberg, D. N., Cowton, T. R., and Sole, A. J.: A model for tidewater glacier undercutting by submarine melting, Geophysical Research Letters, 44, 2360–2368, 2017.

Stevens, L. A., Straneo, F., Das, S. B., Plueddemann, A. J., Kukulya, A. L., and Morlighem, M.: Linking glacially modified waters to catchment-scale subglacial discharge using autonomous underwater vehicle observations, TC, 10, 417–432, 2016.

Straneo, F. and Cenedese, C.: The Dynamics of Greenland's Glacial Fjords and Their Role in Climate, Annual Review of Marine Science, 7, 89–112, 2015.

Veitch, S. A. and Nettles, M.: Spatial and temporal variations in Greenland glacial-earthquake activity, 1993-2010, J. Geophys. Res., 117, F04 007, 2012.

Vieli, A. and Nick, F. M.: Understanding and Modelling Rapid Dynamic Changes of Tidewater Outlet Glaciers: Issues and Implications, Surveys in Geophysics, 32, 437–458, 2011.

Wagner, T. J. W., Wadhams, P., Bates, R., Elosegui, P., Stern, A., Vella, D., Abrahamsen, P., Crawford, A., and Nicholls, K. W.: The "footloose" mechanism: Iceberg decay from hydrostatic stresses, Geophysical Research Letters, 41, 5522–5529, 2014.

Wagner, T. J. W., James, T. D., Murray, T., and Vella, D.: On the role of buoyant flexure in glacier calving, Geophysical Research Letters, 43, 232–240A, 2016.

Wilson, N., Straneo, F., and Heimbach, P.: Satellite-derived submarine melt rates and mass balance (2011–2015) for Greenland's largest remaining ice tongues, The Cryosphere, 11, 2773–2782, 2017.

Xu, Y., Rignot, E., Menemenlis, D., and Koppes, M.: Numerical experiments on subaqueous melting of Greenland tidewater glaciers in response to ocean warming and enhanced subglacial discharge, Annals of Glaciology, 53, 229–234, https://doi.org/10.3189/2012AoG60A139, 2012.